PGC
PUBLISHING

Kuşcu, İ., Yılmazer, E., Demirela, G., Gençalioğlu-Kuşcu, G. and Güleç, N., 2010 - Iron Oxide-(Copper±Gold) Mineralisation in the Turkish Tethyan Collage; *in* Porter, T.M., (ed.), Hydrothermal Iron Oxide Copper-Gold and Related Deposits: A Global Perspective, v. 4 - Advances in the Understanding of IOCG Deposits; *PGC Publishing, Adelaide*, pp. 573-600.

IRON OXIDE-(COPPER±GOLD) MINERALISATION IN THE TURKISH TETHYAN COLLAGE

[1]İlkay Kuşcu, [2]Erkan Yılmazer, [3]Gökhan Demirela, [1]Gonca Gençalioğlu-Kuşcu and [2]Nilgün Güleç

[1]*Department of Geology, Mugla University, Mugla, Turkey*
[2]*Department of Geological Engineering, ODTU, Ankara, Turkey*
[3]*Department of Geological Engineering, Ankara University, Ankara, Turkey*

Abstract - Iron oxide-copper-gold mineralisation within the Turkish Tethyan collage defines a group of diverse, epigenetic copper-gold deposits. As a part of the Tethyan collage, Turkey hosts several IOCG deposits formed in post-collisional, late orogenic, extensional settings, related to subduction of NeoTethyan oceanic crust beneath the Eurasian plate during late Cretaceous to Miocene time. Research on these deposits in Turkey has revealed that some of the iron-oxide mineralisation occurs in metasomatised magmatic rocks that underwent pervasive sodic-calcic and superimposed potassic alteration. These deposits exhibit comparable alteration styles, represented by pre-ore sodic-calcic alteration, overprinted by relatively late syn-ore potassic alteration and magnetite mineralisation, and by post-ore sericitisation and sulphide mineral assemblages. Subsequent alteration, consisting essentially of oxidised sulphides and iron, has in turn been superimposed on the preceding styles. Magnetite is commonly associated with potassic zones, while copper-gold mineralisation accompanies late stage sericitic alteration and carbonatised rocks, mainly along structural discontinuities. The host rocks and alteration are confined to crustal scale regional strike-slip and normal faults.

The Ar-Ar, U-Pb and K-Ar geochronology of minerals from the alteration and magmatic rocks, shows that the interval over which hydrothermal alteration and mineralisation occurred (ca. 74 to 22 Ma), overlaps with the period of calc-alkaline to alkaline magmatism in both the central Anatolian extensional post-collisional, and western Anatolian extensional provinces. The spatial association between the alteration and the magmatic rocks, suggests that the crystallisation and cooling of the Late Cretaceous post-collisional alkaline to calc-alkaline magmatism of central-eastern Anatolia, and the Oligocene-Miocene calc-alkaline magmatism in western Anatolia, contributed to the hydrothermal systems over the entire duration of the metallogenic history of the IOCG provinces. The styles of hydrothermal alteration, mineralogy, paragenesis, stable and radiogenic isotope systematics, and the geochronological data presented here, favour a model in which the fluids responsible for the alteration are largely magmatic. This is further supported by stable and radiogenic isotope data on alteration and associated magmatic rocks.

Based on geochronological evidence and regional compilations, periods favourable for IOCG mineralisation are 74 to 69 Ma in central Anatolia, and 23 to18 Ma in western Anatolia. These intervals are coincident with crustal-scale extension due to post-collisional roll-back of the subducting slab along the Bitlis-Zagros subduction zone (central-eastern Anatolia) and the Aegean subduction complex (western Anatolia). From a Turkish perspective, a demonstration that post-collisional and extensional-intracontinental magmatic settings are fertile for IOCG deposits is critical, as it significantly furthers analogies with both the Canadian 1.9 to 1.5 Ga continental arc settings, and the active, extensional plate margins of the eastern Pacific.

Introduction

The known iron oxide-copper-gold (IOCG) metallogenic districts throughout the world occur both in stable Precambrian shields and on active, extensional plate margins (e.g., Sillitoe, 2003). Information related to deposits in these settings is publicly available in the literature. The IOCG districts of the Tethyan-Eurasian metallogenic belt (TEMB), however, are poorly known, and sparsely distributed, although such mineralisation is known within the belt in Spain, Iran and Turkey. The most prospective settings are located in the Late Cretaceous and Oligocene-Miocene magmatic and metamorphic terranes throughout the TEMB, formed in response to collision between the Afro-Arabian and Eurasian plates, and closure of the NeoTethyan ocean from *ca*. 88 to 20 Ma.Several IOCG deposits in Turkey were formed within post-collisional extensional settings related to this collision. Many of the "potential IOCG districts" in Turkey are under-explored and are poorly known or understood. Although this type of deposit is currently being mined for iron oxides in Turkey, recent work has highlighted their copper-gold potential, and accelerated the exploration for IOCG mineralisation throughout the Turkish Tethyan collage (Kuşcu *et al.*, 2002; Yilmazer *et al.*, 2003; Ay *et al.*, 2005; Kuşcu *et al.*, 2007a, b, c, d).

The appreciation of IOCG mineralisation in Turkey was prompted by the recognition of pervasive sodic and overprinting potassic alteration at the Divriği (Sivas) iron oxide (magnetite-hematite) deposit (Kuşcu *et al.*, 2002; Yılmazer *et al.*, 2003). Research on this deposit (Kuşcu *et al*., 2002; Kuşcu, 2003; Kuşcu *et al*., 2005a) favoured the existence of a distinct family of hydrothermal vein/breccia/replacement Fe±Cu±Au±REE mineralisation in magnetite±copper skarns, characterised by an iron oxide (magnetite and/or hematite) association with 'unusual' sodic and potassic alteration. This has resulted in a growing body of opinion that these deposits are not 'skarn-type', but a distinct deposit class which includes some large to very large ore systems. It has also enhanced the recognition and discovery of similar deposits at Hasançelebi (Malatya), and Şamlı (Balikesir).

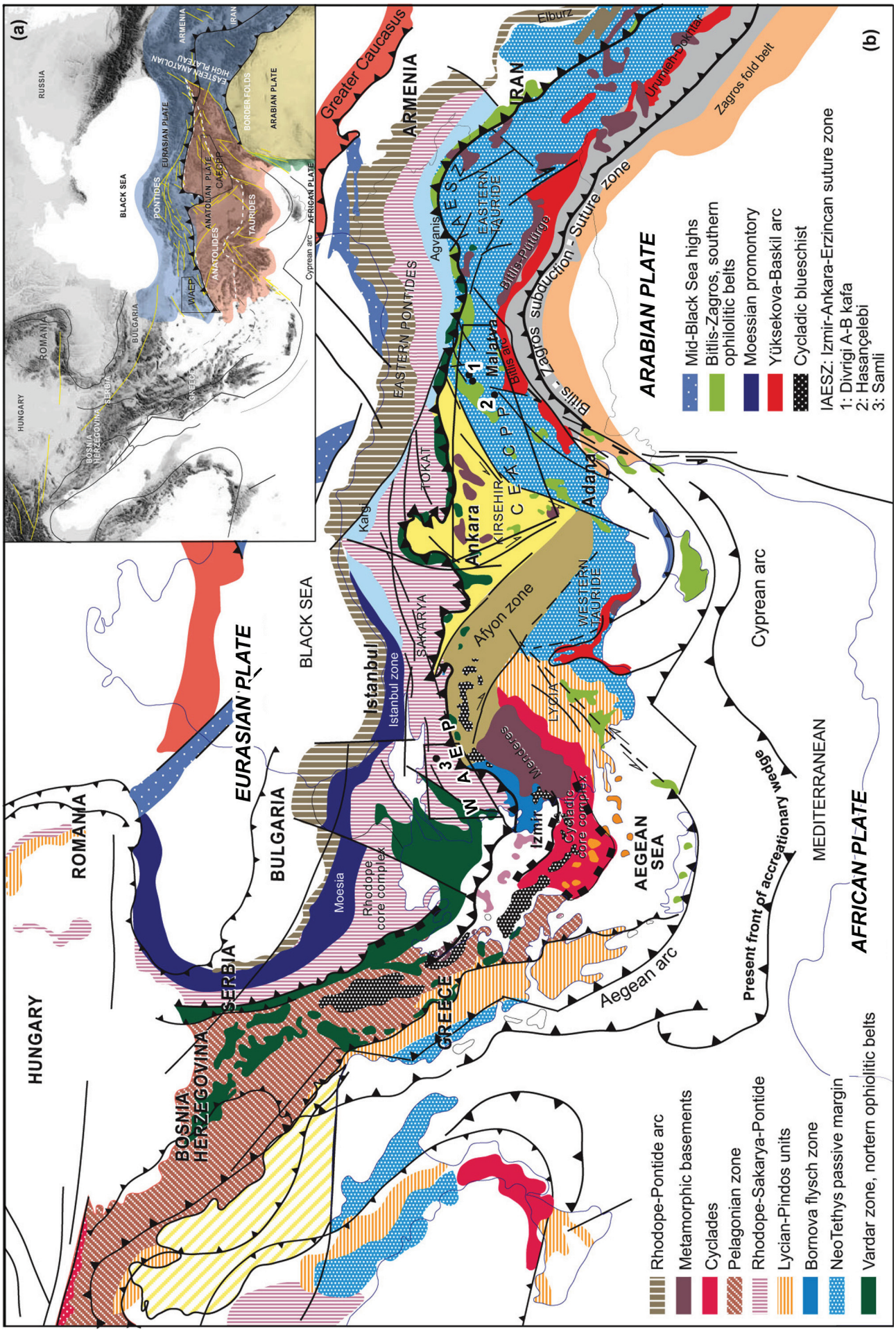
(a)
RUSSIA
ROMANIA
HUNGARY
BULGARIA
GREECE
BLACK SEA
EURASIAN PLATE
ARMENIA
IRAN
ARABIAN PLATE
AFRICAN PLATE
PONTIDES
ANATOLIDES
TAURIDES
BORDER FOLDS
EASTERN ANATOLIAN HIGH PLATEAU
CAUCASUS
WAEP
Cyprean arc
(b)
HUNGARY
ROMANIA
BOSNIA HERZEGOVINA
SERBIA
BULGARIA
EURASIAN PLATE
BLACK SEA
Greater Caucasus
ARMENIA
IRAN
Elburz
Urumieh-Dokhtar
Zagros fold belt
Zagros subduction - Suture zone
Bitlis
Bitlis-Puturge
EASTERN PONTIDES
Agvanis
EASTERN TAURIDE
Malatya
Ankara
KIRSEHIR
Adana
TOKAT
Karg
Istanbul
Istanbul zone
SAKARYA
Afyon zone
WESTERN TAURIDE
LYCIA
Moesia
Rhodope core complex
Izmir
Cycladic core complex
Menderes
AEGEAN SEA
Cyprean arc
Present front of accretionary wedge
Aegean arc
MEDITERRANEAN
AFRICAN PLATE
ARABIAN PLATE
Mid-Black Sea highs
Bitlis-Zagros, southern ophiolitic belts
Moessian promontory
Yüksekova-Baskil arc
Cycladic blueschist
IAESZ: Izmir-Ankara-Erzincan suture zone
1: Divrigi A-B kafa
2: Hasançelebi
3: Samli
Rhodope-Pontide arc
Metamorphic basements
Cyclades
Pelagonian zone
Rhodope-Sakarya-Pontide
Lycian-Pindos units
Bornova flysch zone
NeoTethys passive margin
Vardar zone, nortern ophiolitic belts

Table 1: Geological characteristics of IOCG mineralisation in Turkey (Mgt = magnetite, hem = hematite, py= pyrite, cpy = chalcopyrite).

Deposit name	Related magmatic rocks	Deposit style	Hydrothermal alteration	Main opaque hypogene minerals	Associated metals	Size & grade	Tectonic setting	Age (Ma) host rocks / alteration
Divriği A-B Kafa (Sivas)	Monzonite, monzodiorite, diorite	Veins, replacement & pockets	Early scapolite-garnet-diopside; middle phlogopite-K feldspar; late sericite-quartz-calcite.	Mgt. hem. py. cpy	Co, Ni, U, Ba, F, LREE	133.8 Mt @ 56% Fe, 0.5% Cu	Post-COLG exhumation	77-62 / 73.5
Hasançelebi (Malatya)	Dolerite, microsyenite-porphyry, trachyte	Veins, disseminations	Early scapolite-garnet-diopside-actinolite; middle phlogopite-K feldspar; late sericite-quartz-calcite-barite.	Mgt. hem. py. cpy	U, Ba, LREE, F, Au	94.8 Mt @ 23% Fe_3O_4, 0.8-2.75% Cu, 1.9% Ni, 0.04-2 g/t Au	Post-COLG, late orogenic, within plate	76.8-69.9 / 74.2-68
Şamlı (Balikesir)	Granodiorite, granite, diorite	Veins, replacements	Early albite-garnet; middle K feldspar; late epidote-sericite-quartz.	Mgt. hem. py. cpy	Bi, Co, Ni, LREE, native Cu	NA	Core complex	23.5-22 to 18.4 / NA

The results of the work detailed above, and other recent research on a diverse group of Fe-skarn and IOCG mineralised occurrences in Turkey, including material synthesised from unpublished research reports and theses, are used to provide an insight into metallogenic processes and evolution of IOCG deposits in the Turkish Tethyan collage. IOCG-style deposits, are here considered to be those with either: (1) hydrothermal, monometallic, low-titanium magnetite and/or hematite accompanied by elevated copper±gold (i.e., those in which iron is the sole significant metal), or (2) polymetallic iron deposits typically accompanied by pervasive Na-Ca and K-Fe alteration, with associated Cu (±Au) REE, U, Ba, and F occurring as significant economic commodities. In this contribution, we review salient features of the alteration styles, temporal and spatial relationships between mineralisation, alteration and magmatism; and the geological-geochemical, geochronological, available radiogenic and stable isotope systematics, along with metallogenic settings of the IOCG-style deposits of Turkey. The review relates specifically to the Western Anatolian Extensional Province (WAEP) (Şamlı deposit) and Central-Eastern Anatolian Collisional-Post Collisional Province (CEACPP) (Hasançelebi and Divriği deposits; Fig. 1; Table 1). It also reviews the regional and local geological features, and the tectonic and metallogenic setting of known examples of Turkish IOCG-style mineralisation, and focuses on some key features that can help to unveil prospective iron oxide deposits, with notable copper-gold mineralisation, formerly regarded as skarn-type.

Figure 1 (facing page). (a) Digital elevation map of Turkey illustrating the major microcontinental fragments and the Eurasian, Afro-Arabian plates, **(b)** Correlation of Tethyan belts in the western Tethysides with respect to major suture zones and terrains in Turkey (Modified from Stampfli, 2001; Jolivet, *et al.*, 2004, and Kaymakci and Kuşcu., 2007), and location of the WAEP and CEACPP.

Geological Setting

General Features of the Turkish Tethyan Collage

The age and distribution of geological events in Turkey are directly related to the existence and closure of a westward narrowing embayment of the Tethyan Ocean that separated Laurasia and Gondwana since the Carboniferous (Şengör and Yılmaz, 1981). This ocean opened and closed over two different periods during its evolution as the Palaeo- and NeoTethys respectively (Şengör, 1987; Stampfli, 1996). Many alternative models have been proposed for the evolution of these oceans in Turkey, differing mainly in the timing of opening and closure, subduction polarity, and the location and number of sutures (Şengör and Yılmaz, 1981; Okay and Tüysüz, 1999; Göncüoğlu *et al.*, 2000; Stampfli, 2001; Bozkurt and Mittwede, 2001). However, as part of the greater Alpine-Himalayan Belt, the geodynamic evolution and present geological framework of Turkey is predominantly related to the closure of the younger NeoTethys ocean, and collision of the Eurasian and Afro-Arabian plates during the Mesozoic to Cenozoic Alpine orogeny. During this closure of the Neotethys, a suite of micro-continental fragments (Figs. 1a and b) (Şengör and Yılmaz, 1981; Göncüoğlu *et al.*, 1997; Okay and Tüysüz, 1999) were formed; comprising from north to south, the (1) İstanbul, (2) Sakarya, (3) Bornova Flysch and (4) Afyon Zones, and the (5) Menderes Massif (Okay and Tüysüz, 1999; Bozkurt and Oberhänsli, 2001; Bozkurt and Mittwede, 2001). These are also grouped to include the major terrains from north to south as the Pontides, Tauride-Anatolide Block, Border Folds (Southeastern Anatolian orogenic belt-Arabian Platform) and Eastern Anatolian accretionary prism (Eastern Anatolian high-plateau; Ketin, 1966; Şengör and Yılmaz, 1981; Şengör *et al*., 1984; Fig. 1a). The terminal closure and final amalgamation of these fragments took place during the Late Tertiary when the Arabian and Eurasian plates collided (Anatolian microplate *sensu stricto*). The Central-Eastern Anatolian Collisional-Post Collisional Province (CEACPP) and Western Anatolian Extensional Province (WAEP) are respectively located on the eastern and western parts of the Tauride-Anatolide block (Figs. 1a and b). The CEACPP and WAEP incorporate major Late Cretaceous to Miocene-Pliocene magmatic complexes which are sequential arc to post-collisional and late-orogenic volcano-plutonic products, and were emplaced into broadly deformed metasedimentary, ophiolitic and sedimentary units of Palaeozoic to Mesozoic and Cenozoic ages.

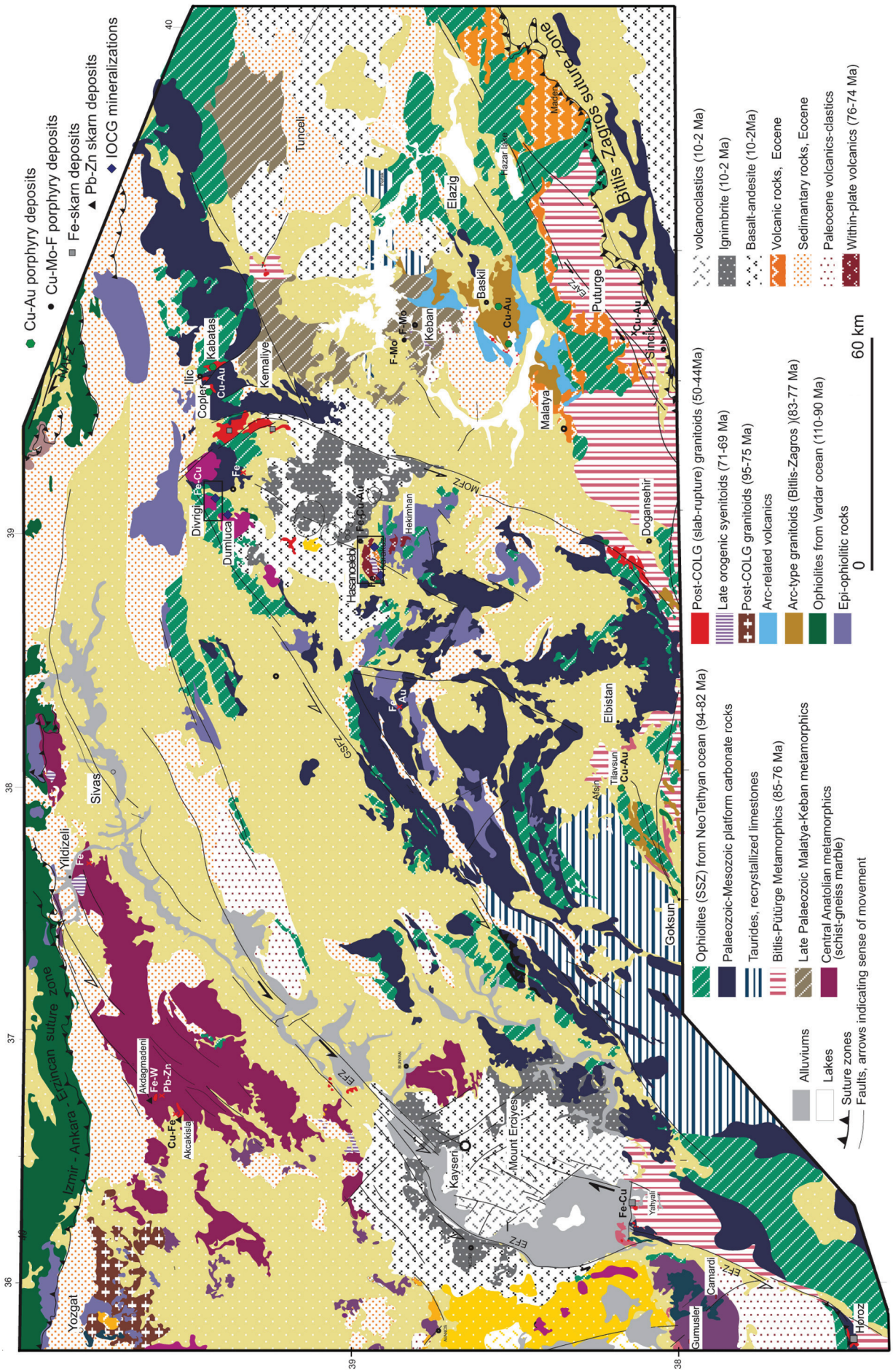

Figure 2: Simplified geological map of the Baskil-Divrigi province (MOFZ = Malatya-Ovacik fault zone; EAFZ = East Anatolian fault zone; NAFZ = North Anatolian fault zone; GSFZ = Yakapinar-Göksu-Sarız fault zone; EFZ = Ecemiş (Central Anatolian) fault zone. Rectangular outlines show the location of the Divriği and Hasançelebi IOCG-style deposits.

The latest Cretaceous (94.5 to 69.0 Ma; Boztug *et al*., 2007; Kuşcu *et al.*, 2007a, 2008) to Quaternary igneous activity emplaced intrusive rocks into the metamorphosed platform carbonates and overlying ophiolites (Figs. 2 and 3) of the CEACPP. This magmatism is generally considered to have taken place under variably extensional conditions in response to retreating subduction boundaries (slab roll-back) and initial slab rupture (Kuşcu *et al.*, 2007a; 2008) to slab break-off (Şengör *et al*., 2003; Keskin, 2003) along the Bitlis-Zagros subduction zone. The known IOCG and iron-skarn type mineralisation in the CEACPP is found in the Divriği (Sivas) and Hasançelebi (Malatya) districts where Late Cretaceous to Eocene granitoids are emplaced into Late Cretaceous sedimentary and metasedimentary sequences (Kuşcu *et al.*, 2008) (Fig. 2).

The Fe-skarn and IOCG-style mineralisation of the WAEP is hosted by, or is associated with, Late Oligocene to Early Miocene volcano-plutonic complexes (23-22.3 to 18 Ma; Ataman, 1974; Watanabe *et al.*, 2003; Isik *et al*., 2004; Ring and Collins, 2005, Innocenti *et al.*, 2005; Fig. 4). These complexes are generally accepted to have been formed during orogenic collapse (Bozkurt and Park 1997; Wortel and Spakman, 2000; Okay and Satir, 2000; Bozkurt, 2001; Doglioni *et al*., 2002; Innocenti *et al.*, 2005) due to slab roll-back along the Aegean subduction complex. Extensive east-west to northeast-southwest oriented brittle fault systems in central Anatolia (Fig. 2), and/or ductile/brittle shear zones and deeply penetrating detachment faults trending east-west to northeast-southwest in western Anatolia, are the main pathways for the emplacement/exposure of the causative calc-alkaline and alkaline magmatism (Fig. 4).

Mineral Deposits and Iron Oxide-(Cu±Au) Mineralisation of the CEACPP

The CEACPP (Central-Eastern Anatolian Collisional-Post Collisional Province) contains iron-, iron-tungsten and lead-zinc skarns, copper-gold to fluorine-molybdenum-copper porphyry mineralisation, epithermal antimony-mercury-gold deposits and IOCG-style mineralisation. Baskil (Elaziğ) and Copler (Erzincan) are major districts comprising Late Cretaceous to Early-Middle Eocene molybdenum-gold and copper-gold porphyry mineralisation, with recently commenced mining operation at Copler. (Kuşcu *et al*., 2007b; Fig. 2). Within the province, Celebi, Kesikkopru, Durmuslu (Kırsehir), Karamadazı (Kayseri), Dedeyazi (Malatya) and Bizmisen, Otlukilise (Sivas) exploit important Fe-skarns with significant copper enrichment. All are spatially and genetically associated with Late Cretaceous to Middle Eocene magmatic rocks (Kuşcu *et al.*, 2007b). Within this province, Akcakısla, Akdağmadeni (Yozgat) are still operating, while Keskin (Kırıkkale) and Keban (Elaziğ) are abandoned lead-zinc skarn deposits. Huseyinbeyobası (Kırıkkale) is a currently exploited vein-type molybdenum deposit. Bayındır, Akcakent (Kırşehir) and Keban (Elaziğ) are vein-type epithermal fluorine and fluorine-molybdenum-copper porphyry occurrences, hosted by Late Cretaceous alkaline intrusions. Gumusler and Madsan (Nigde) are abandoned epithermal antimony-mercury and gold deposits with notable tungsten and tin enrichments that are related to aplitic to pegmatitic Late Cretaceous granitoid intrusions.

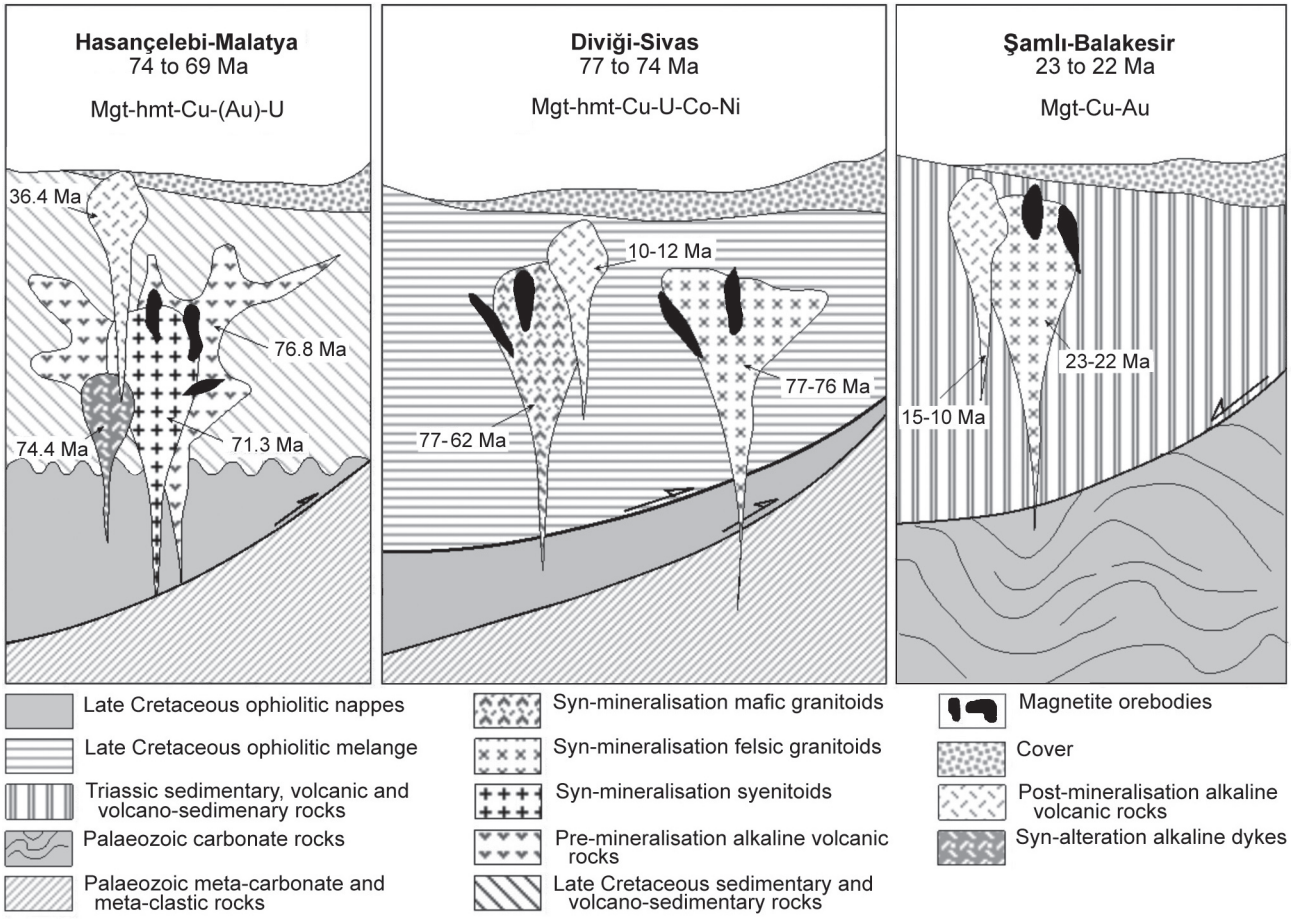

Figure 3: Diagrammatic representation of the geological environments of Turkish iron oxide-copper-gold occurrences (Mgt: magnetite, hmt: hematite).

Table 2: Selected samples from the Murmano pluton (samples from MG-2 to 9 are from Boztuğ *et al.*, 2007). nd = not detected. na = not analysed.

	Felsic								**Mafic**					
Sample	338	340	452	454	457	MG1	MG2	MG4	MG3	MG5	MG6	MG7	MG8	MG9
SiO_2	58.96	58.47	64.09	65.47	58.91	69.76	68.87	62.81	46.68	46.11	52.53	53.2	45.54	47.89
Al_2O_3	17.98	18.08	17.33	16.76	17.65	15.34	16.08	17.42	18.86	15.67	18.87	18.92	13.35	15.83
Fe_2O_3	5.07	5.48	2.59	3.50	4.62	na	na	na	na	na	na	na	na	na
CaO	4.29	4.43	2.84	2.67	4.63	1.83	2.08	3.24	13.39	12.96	7.41	7.66	15.27	13.48
MgO	2.15	2.20	1.30	1.30	2.65	0.73	0.62	1.72	6.08	7.4	3.44	3.54	6.46	7.3
Na_2O	4.64	4.16	3.88	3.76	4.13	3.99	4.34	4.34	3	2.56	4.69	4.11	2.67	2.57
K_2O	4.91	4.76	5.61	5.02	4.59	4.59	4.66	4.93	1.41	1.92	3.75	3.64	2.2	1.98
TiO_2	1.08	1.19	0.63	0.52	1.05	0.26	0.25	0.65	1.41	1.33	0.95	0.92	1.82	1.21
MnO	0.04	0.04	0.02	0.02	0.04	0.01	0.01	0.03	0.09	0.16	0.11	0.11	0.16	0.13
P_2O_5	0.32	0.35	0.21	0.19	0.36	0.18	0.11	0.17	0.42	0.49	0.35	0.37	1.07	0.18
Fe_2O_{3T}	7.62	8.50	3.80	5.17	6.93	1.75	1.9	3.74	6.97	10.31	6.59	6.56	10.42	3.63
FeO	2.55	3.02	1.21	1.67	2.31	na	na	na	na	na	na	na	na	na
LOI	0.44	0.52	0.68	0.46	0.84	1.2	0.8	0.7	1.4	0.8	1	0.7	0.7	0.5
TOTAL	100.05	99.86	99.33	99.81	99.62	99.77	99.84	99.9	99.83	99.83	99.82	99.85	99.8	99.82
Ba	1215	1330	975	914	1080	1027	1029	1243	844	669	1102	1003	1089	635
Rb	153.00	162.00	160.50	161.50	136.00	165.1	136.1	154.9	49.5	64.8	157.4	249.8	82.1	66.8
Sr	352	389	311	302	380	196.4	234	340.1	927.8	703.5	547.7	566.7	472.6	588.2
Cs	1.58	1.98	1.35	1.38	1.46	2	1.5	1.4	1.4	2.2	10.4	8.7	5	2.8
Ga	20.30	20.60	19.60	19.40	20.30	21.2	20.2	22.5	18.8	17.5	19.9	17.6	19.1	16.4
Ta	2.40	2.10	2.70	2.50	2.00	2.9	1.7	1.9	1.1	1.1	1.8	0.9	1.4	1
Nb	37.00	31.90	29.10	26.80	30.90	17.2	14.8	23.8	14.9	13.6	21.2	11.5	20	12.2
Hf	5.50	4.60	4.80	6.40	7.20	3.3	3.1	4.2	2.4	2.6	3.7	2.6	4.8	3.5
Zr	224.0	188.5	186.5	257.0	303.0	103.3	110.2	149.8	74.9	107.1	159.9	99.9	195.7	122.2
Y	29	30	26	23	31	13.4	43.3	15.8	23	19.9	21.3	18.8	34.7	20.5
Th	22.8	23.5	30.5	28.4	21.2	7	12.8	16.8	2.5	4.1	10.1	5.8	10.5	6.5
U	7.77	6.04	7.50	8.29	5.86	4.7	4.2	4.8	0.6	2.1	4.9	2.6	6.3	2.4
Cr	30	30	30	30	50	nd	nd	nd	nd	nd	nd	nd	nd	nd
Ni	12	13	15	15	41	12.6	2.9	14	38.4	67	26.4	22.7	29.5	78.5
Co	9.0	9.8	5.7	6.9	15.8	186.7	94.2	72.3	59.2	58.6	49	45	52.8	58
V	98	108	67	57	106	20	24	56	207	236	118	113	284	202
Cu	7	10	5	5	26	1.8	1.2	8	1.9	26.1	34.1	36.1	27.7	26.8
Pb	13	30	10	16	11	1.9	2	6.1	3	1.9	2.6	2	4	2.9
Zn	44	72	32	41	39	6	5	15	34	61	67	63	44	50
Sn	2	2	5	3	4	3	4	2	2	2	2	nd	1	
W	2	4	3	5	1	1078.1	700.3	488.6	260.9	184.2	253.1	207	154.8	220.9
Mo	2	2	2	2	nd	nd	nd	0.1		1.2	3.2	3.6	0.8	1.8
La	40.0	44.9	43.6	36.7	45.8	17.7	21.5	24.7	25.1	22	36.1	33.7	44.6	18.3
Ce	77.2	93.9	87.6	69.8	95.6	32.9	41.1	57.8	57.4	42.7	63.1	58.2	84.5	37.1
Pr	8.75	10.95	9.87	7.60	11.10	3.98	4.58	5.48	6.58	4.87	6.97	6.6	10.09	4.59
Nd	33.80	39.70	34.90	26.50	39.70	15.3	15.6	20.2	28.2	21	26.5	24.2	39.4	19.8
Sm	6.45	6.90	6.24	4.76	7.36	2.5	2.9	3.5	4.4	3.4	4.4	3.8	7.1	3.8
Eu	1.36	1.45	1.22	0.92	1.47	0.79	0.77	1.08	1.65	1.36	1.47	1.27	1.75	1.2
Gd	6.24	6.58	6.06	4.38	7.00	2.47	2.1	2.96	4.89	3.35	4.06	3.32	6.57	4.25
Tb	0.88	0.92	0.83	0.69	0.94	0.37	0.35	0.41	0.73	0.64	0.6	0.66	1.08	0.58
Dy	5.23	4.98	4.48	3.54	5.08	2.2	2.08	2.55	3.68	3.07	2.98	3.3	5.41	3.25
Ho	1.03	0.98	0.88	0.73	1.06	0.43	0.41	0.49	0.79	0.67	0.71	0.63	1.14	0.71
Er	3.10	2.93	2.69	2.27	3.02	0.98	1.12	1.39	2.03	1.94	2.04	1.89	3.24	1.96
Tm	0.41	0.42	0.38	0.32	0.44	0.18	0.18	0.21	0.33	0.26	0.33	0.28	0.47	0.32
Yb	2.91	2.94	2.65	2.27	3.04	1.04	1.21	1.76	1.99	1.88	2.21	1.81	2.77	1.93
Lu	0.46	0.40	0.40	0.37	0.44	0.17	0.18	0.26	0.34	0.28	0.36	0.23	0.47	0.32

In addition to the Kiruna-type magnetite-apatite ores at Avnik (Bingol, southeastern Turkey), it is suggested that several of the iron-oxide deposits in the CEACPP represent IOCG-style mineralisation (e.g., Stendal *et al.*, 1995; Stendal and Unlu, 1991; Unlu and Stendal, 1989; Kuşcu *et al.*, 2002, 2005, 2007a, 2007b; Yılmazer *et al.*, 2003; Ay *et al.*, 2005). Divriği A-B Kafa (Sivas) and Hasançelebi Karakuz (Malatya) are iron-oxide ±copper ±gold occurrences containing zones of up to 2 ppm Au and 2% Cu. The characteristics of these IOCG-style occurrences are shown in Table 1. For many years, these deposits have been exploited for iron, while the late stage sericite, silica and carbonate altered rocks, with abundant sulphides (mainly pyrite, malachite and marcasite), were discarded onto the dumps and into the tailings dam.

Divriği (Sivas) IOCG Mineralisation

Local Geology

Two discrete mineralised bodies are found at Divriği (Sivas); A- and B-Kafa (resources of 133.8 Mt with 56% Fe and 0.5% Cu; Koşal, 1973). Both are within a host sequence which includes the Munzur limestones, and serpentinised ultramafic rocks of the Günes ophiolite, intruded by the Murmano and Dumluca plutons (Fig. 3; Figs. 5a and b). The A- and B-Kafa ore bodies represent two end-members of the same hydrothermal system at Divriği (Figs. 5b). At A-Kafa, high temperature Na-Ca and K-Fe alteration is associated with the main magnetite mineralisation (Fig. 5b), while at B-Kafa, late alteration, formed at relatively low to moderate temperatures, accompanies hematite, limonite

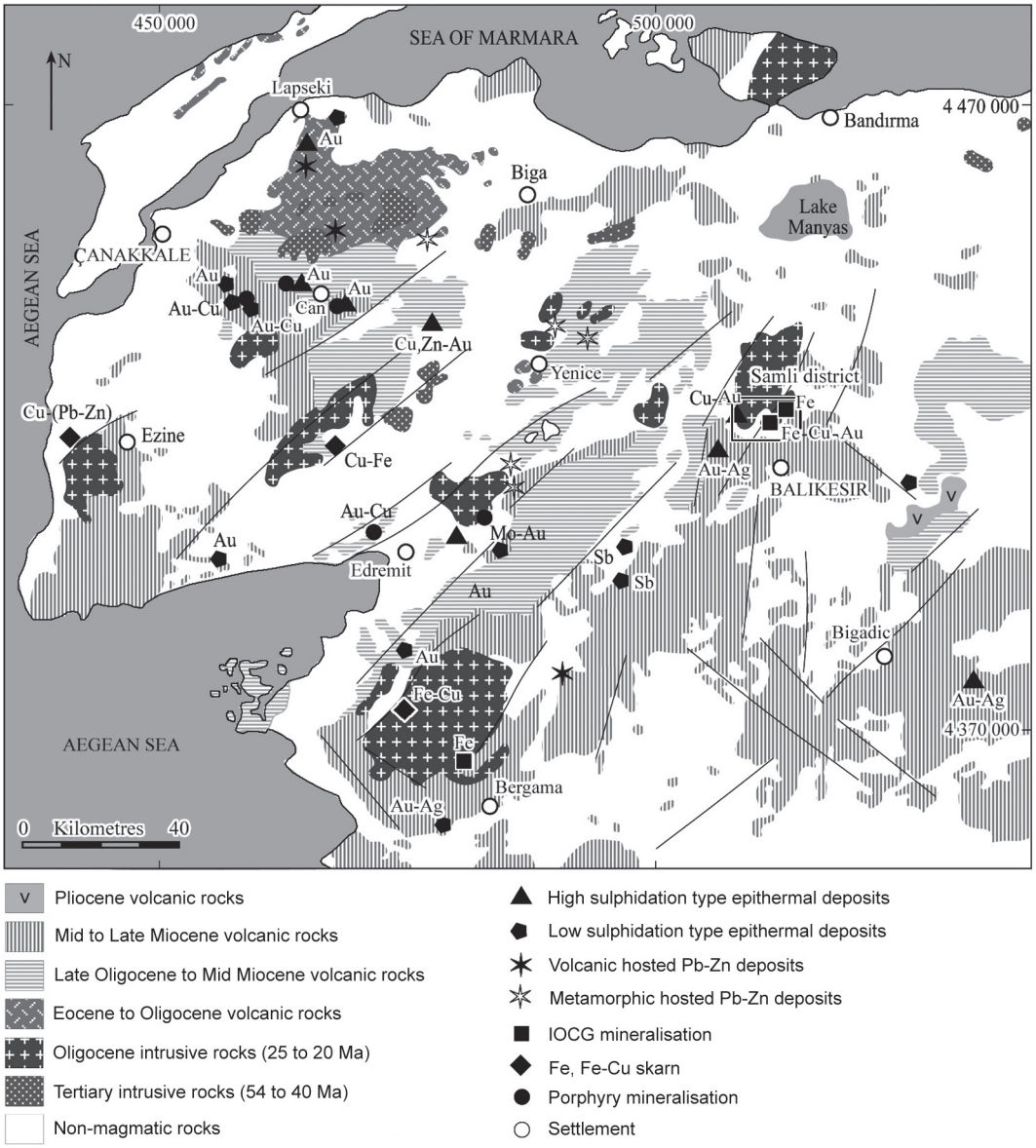

Figure 4: Simplified geological map of the western Anatolian extensional province showing the location and distribution of the mineralisation; frame shows the location of the Şamlı IOCG mineralisation.

and sulphide mineralisation (Yılmazer *et al*., 2003). The contact between the two is defined by an ENE-WSW trending strike-slip fault with a reverse displacement (Figs. 5a and b). The B-Kafa body is predominantly hosted by carbonate blocks within the ophiolitic mélange at their contact with plutonic rocks (Fig. 5b). As no direct analyses have been undertaken for gold, its presence in significant quantities is debatable. Consequently, the alteration and mineralisation in Divriği could be classified as a magnetite-hematite-rich end-member of the IOCG-style with notable copper mineralisation.

The Munzur Limestone of Early Carboniferous to Campanian (Late Cretaceous) age (Öztürk and Öztunali 1993; Yılmaz *et al.*, 2001) represents the lowermost unit in the Divriği area (Figs. 5a and b). It occurs below the obducted rocks of the Güneş ophiolite, which were rooted to the northerly NeoTethyan oceanic crustal rocks. These ophiolites comprise serpentinised ultramafic rocks, layered cumulate and isotropic gabbro, and sheeted dykes (Parlak *et al.*, 2006). Late Cretaceous volcanosedimentary rocks (the Campanian-Maastrichtian Saya formation; Yılmaz *et al.*, 2001), comprising clastic and volcaniclastic sequences, unconformably overlie the ophiolites (Fig. 5a). The Late Cretaceous to Early Paleocene (Campanian to Danian) Murmano and Dumluca plutons (Boztuğ and Harlavan 2007), mainly cut the Late Cretaceous ophiolites, but also in part, the Munzur limestone (Figs. 5a and b). Numerous aplite, lamprophyre and dolerite dykes intrude the plutonic and ophiolitic rocks. The cover sequence at Divriği is Eocene to Pliocene-Pleistocene in age and consists of epiclastic conglomerates, carbonate rocks, evaporites and volcanic rocks. The uppermost sequence covering the whole area is the Pliocene to Quaternary volcanic-volcaniclastic succession of the Yamadag volcanics (Fig 5a).

Geochemistry and Petrogenesis of Magmatic Rocks

The Murmano pluton has felsic and mafic end-members (Table 2; Figs. 6a and b). These are calc-alkaline to alkaline, metaluminous, and exhibit high-K characteristics, although highly differentiated members of the felsic suite are transitional to peraluminous in character (Boztuğ *et al.*, 2007) (Figs. 6b and c). Kuşcu *et al.* (2005a) showed that the alkalinity of the granitoids at Divriği is due to a secondary process that may be related to alkaline metasomatism

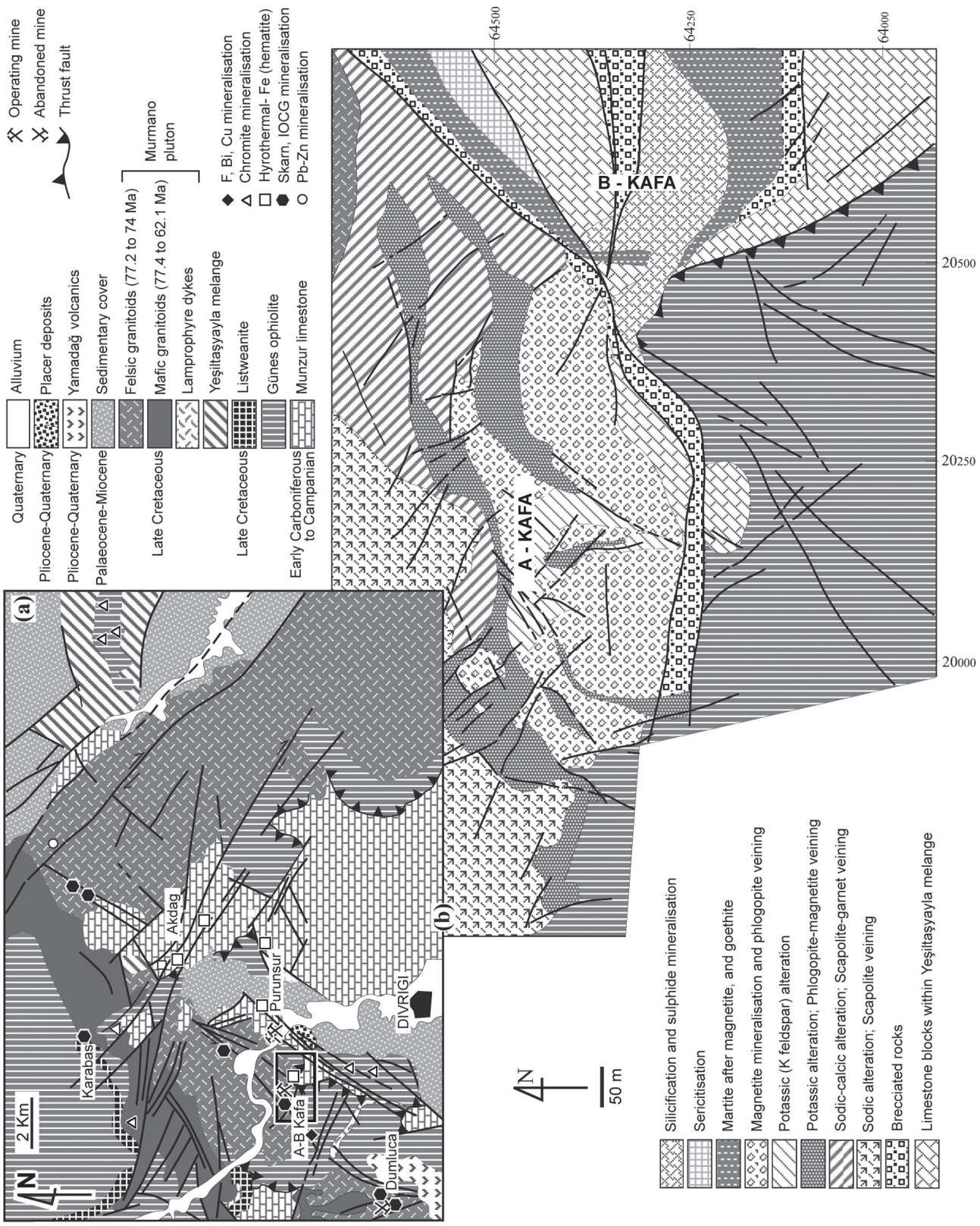

Figure 5: Geological map of **(a)** Divriği (Sivas) region (Modified from Öztürk and Öztunalı, 1993, and Boztuğ, *et al.*, 2007), and **(b)** the A-B Kafa mineralisation in the framed area shown on (a) (Modified from Yılmazer, *et al.*, 2003)

associated with the IOCG-style mineralisation in the area. The rocks of the felsic and mafic end-members are classified as granodiorite to monzonite, and monzogabbro, gabbro, diorite to quartz-diorite, respectively (Fig. 6d). The LREE and LIL elements are enriched with respect to HREE and HFS elements (Figs. 7e and f). The granitoids show negative Eu and Nb, and positive Rb, Th and La anomalism (Fig. 7f). LREE and HREE patterns of felsic and mafic end-members, favour derivation from separate, but coeval, mafic and felsic magma sources (Figs. 6e and f), typical of hybrid magmas (Boztuğ *et al.*, 2007). They are transitional from WPG (within-plate granite) and VAG (volcanic arc granite) to syn-COLG (collisional granite) settings (Fig. 6g; Pearce, 1984). They have low to moderate Nb/Th ratios, suggestive of a transition from arc to OIB (ocean island basalt) + MORB (mid ocean ridge basalt) settings, indicating crustal contamination (Figs. 6h and j) or a metasomatised mantle source. In general, the geochemical trend of the granitoids is more akin to that of arc granites and A-type felsic rocks that show a linear distribution between OIB and IAB (island arc basalt; Fig. 7i). The multi-element patterns of felsic and mafic end members in spider- and REE diagrams, in conjunction with Th/Yb vs Ta/Yb, Yb/Ta vs Y/Nb and Ba/Nb vs La/Nb, suggest assimilation and/or combined fractional crystallisation played an important role in magma generation (Figs. 6j, k and l). The initial $^{87}Sr/^{86}Sr$ and $^{143}Nd/^{144}Nd$, stable and some radiogenic isotope ratios (Boztuğ *et al.*, 2007) are suggestive of an enriched mantle (EM-II type) source for the mafic magma, modified by subduction-derived elements. Likewise, lower Nb/Th, along with negative Nb anomalies (Fig. 6j) and increasing Ta/Yb with Th/Yb ratios (Fig. 6k) favour an enriched mantle or a metasomatised mantle source for the granitoids. Boztuğ *et al.* (2007) concluded that the igneous activity in the district was derived from two different, but coeval magma sources; one an EM II type of mantle-derived mafic variety, the other a hybrid felsic product generated by mixing of mantle- and crustal-derived melts; and that the Murmano pluton magma assimilated significant crustal material during ascent.

The generation of these granitoids has been linked to either: (1) extension, driven by slab roll-back of the oceanic lithosphere along the Bitlis-Zagros suture zone (southerly NeoTethyan ocean), which resulted in an invasion of hot asthenosphere (Kuşcu *et al*., 2007a), or (2) the slab break-off stage of the NeoTethyan convergence system along the Izmir-Ankara-Erzincan suture zone (e.g., Boztuğ and Harlavan, 2007; Boztuğ *et al*., 2007). The timing of continental collision in Turkey took place roughly by the end of the Oligocene, and the subducting slab should have broken-off at around 12 Ma (Hafkenscheid *et al.*, 2006). Although the timing of slab break-off agrees with other studies (Kohn and Parkinson, 2002, Keskin, 2003; Sengor *et al.*, 2003; Fascenna *et al.*, 2006; Hafkenscheid *et al.*, 2006; Angus *et al.*, 2006), a lower convergence velocity of the Arabian plate would have led to a locally later break-off (Van de Zedde and Wortel, 2001). If continental collision began at approximately 22 Ma in the Arabian region, the slab would have broken off at around 12 Ma (Van de Zedde and Wortel, 2001). Consequently, a slab break-off model for the generation of granitoids in the Divriği district is unlikely. It is therefore suggested that these granitoids were formed over a prolonged period of extension within the overriding plate (Anatolian microplate), related to slab roll-back during the closure of the NeoTethyan ocean (Kuşcu *et al.*, 2007a).

Geochronology

Ar-Ar geochronology of magmatic biotite from monzonite-monzodiorite gave ages of 73.50±0.40 to 73.48±0.40 Ma (Table 3; Kuşcu *et al.*, 2007b; 2008). K-Ar geochronology of magmatic hornblende and/or biotite, yield cooling ages ranging from 76.6±0.6 to 77.2±1.8 Ma for the felsic, and from 77.4±1.5 to 62.1±0.3 Ma for mafic end-members of the Murmano pluton (Boztuğ *et al.*, 2007). Ar-Ar dating of phlogopite from K-Fe altered rocks returned ages of between 73.40±0.39 and 74.34±0.8 Ma (Table 3). Hydrothermal biotite from K-Fe altered rocks at A-Kafa gave identical weighted mean plateau ages of 73.75±0.62 and 74.34±0.83 Ma (Marschik *et al.*, 2008) suggesting a minimum age for the potassic alteration and magnetite ore. The K-Ar geochronology of Murmano mafic and Ar-Ar geochronology of phlogopite/biotite from the K-Fe alteration (Kuşcu *et al.*, 2007b) collectively favour a temporal genetic relationship between emplacement of the Murmano mafic end-member and alteration/mineralisation.

Table 3: Ar-Ar. U-Pb and K-Ar geochronology on selected magmatic rocks in the CEACPP (Shown are weighted mean or plateau and concordia ages; dates in italics refer to the age of alteration/hydrothermal minerals). Sources: 1 - Boztuğ *et al*., 2007; 2 - Marschik *et al*., 2008; 3 - Kuşcu *et al*., 2008.

Magmatic rock/pluton		Rock type	Ar-Ar ages			U-Pb	K-Ar
			Hornblende	Biotite	K feldspar	Zircon	Biotite-hornblende
Post-collisional extension, roll back	Divriği	Quartz syenite					76.6±0.6[1]
		Granite		*73.75±0.6*[2]			77.2±1.8[1]
		Monzonite-monzodiorite		73.48±0.40 [3] *74.34±0.8*[2]			
		Monzonite-monzodiorite		73.50±0.40[3]			
		Granite with biotite phenocrysts		*73.40±0.39*[3]			
		Trachyte-trachyandesite		76.84±0.6[3]			
Late orogenic-within plate	Hasançelebi	Syenite porphyry			70.48±0.42[3]	71.3± 0.5[3]	
		Dolerite dyke	74.40±0.51[3]	74.32±0.4[3] *74.26±0.45*[3]			
		Syenite porphyry. intruding ophiolites				69.0± 0.4[3]	
		Syenite feldspar porphyry			*70.48±0.4*[3] *68.64±0.4*[3]	71 ± 1[3]	

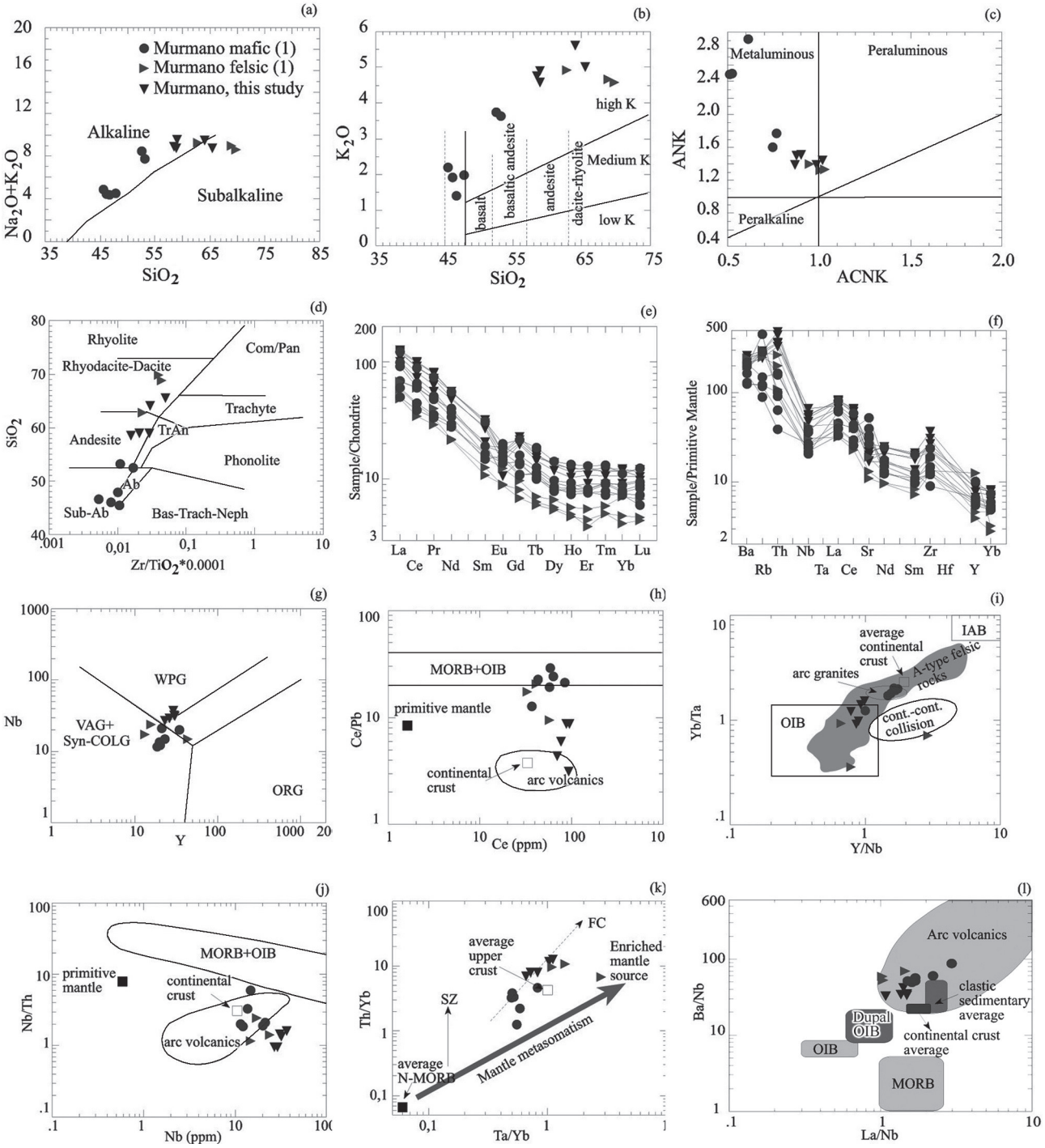

Figure 6: Geochemical classification and discrimination diagrams for the Murmano pluton within the Divriği district: **(a)** Total alkalis vs. silica (Irvine and Baragar, 1971); **(b)** K_2O vs. silica (Le Maitre, *et al.*, 1989); **(c)** Shand index; **(d)** compositions of granitoids (Winchester and Floyd, 1977; 1: data from Boztuğ, *et al.*, 2007); **(e)** Chondrite-normalised REE; and **(f)** Prim (primordial mantle)-normalised spider diagrams (Normalisation values after Sun,1982); **(g)** tectonic setting of granitoids (Pearce, 1984); **(h)** Ce/Pb vs. Ce; **(i)** Yb/Ta-Y/Nb diagram (Best and Christiansen, 2001; Whalen, *et al.*, 1987) diagram showing the effect of crustal contamination and within-plate signature; **(j)**, Nb/Th vs. Nb plots for granitoids (primitive mantle after Hofmann (1988); continental crust, MORB (mid-ocean ridge basalts), OIB (ocean-island basalts), IAB (island arc basalts), arc volcanics compositions were taken from Schmidberger and Hegner, 1999). The compositions of MORB, OIB, IAB and CC (continental crust) were taken from Taylor and McLennan (1985); **(k)** Th/Yb vs Ta/Yb diagram (Pearce, 1983) showing the effect of mantle metasomatism; and **(l)** Ba/Nb-La/Nb diagram (Jahn, *et al.*, 1999).

Alteration

Altered carbonate blocks within the ophiolite suite exhibit very limited skarn developments, up to a few metres thick, consisting of green to brown garnet with no associated mineralisation, mainly outside of the A- and B-Kafa orebodies. The ophiolites have only undergone minor to very rare alteration, occurring mainly as hydrothermal biotite and occasional epidote, commonly along fracture zones close to the granitoid contact. The plutonic rocks were subjected to early, pre-ore, pervasive Na-Ca alteration that produced an assemblage of garnet-diopside and scapolite, followed by a syn-ore K-Fe episode overprinting the former. The Na-Ca alteration occurs as either parallel, northeast-southwest trending veins of scapolite or garnet-diopside-scapolite, or as irregular scapolite pockets or replacement bodies, no more than 150 cm across, within monzonitic to monzodioritic rocks. The garnet and diopside are not pervasive, as compared to scapolite, and occur either alone, as individual 2 to 5 cm thick veins, or as veins with associated <10 cm thick scapolite veins on their margins. These veins are mainly distal to the main magnetite ore

(Fig. 5). No magnetite and/or hematite mineralisation is associated with Na-Ca alteration or scapolite and garnet-diopside-scapolite veining.

K feldspar and phlogopite are the dominant constituents of the K-Fe alteration. They are found proximal to the magnetite ore, occurring as northwest-southeast trending veins cross-cutting or superimposed upon the scapolite, garnet-scapolite veining, and are controlled by faults of the same orientation that off-set the Na-Ca altered rocks. The development of northwest-southeast faulting and fracturing was coeval with hydrothermal brecciation of the plutonic rocks, and the formation of phlogopite and K feldspar veining. The thickness and intensity of phlogopite veining is related to the degree of fracturing and brecciation of the monzonitic rocks and Na-Ca altered zones. The thickest phlogopite veins and replacements (up to 30 m across) are hosted by the most intensively fractured and sheared rocks that had previously undergone Na-Ca alteration.

The magnetite mineralisation is coeval with, or slightly post-dates, the generation of phlogopite. The orebodies occur as veins of up to 10 to 15 m in thickness, or as replacement bodies and pockets ranging in size from a few cm to 20 to 30 m across, within the K-Fe alteration zone. Late-alteration includes post-ore phases hosting sulphide, and maghematised and martitised magnetite and hematite, and later sericite-calcite-barite and quartz. The latter occurs close to the surface, or in the upper sections of the hydrothermal system within the B-Kafa body. The sulphides accompanying iron oxides include disseminated pyrite, marcasite and chalcopyrite. Chalcopyrite has been oxidised to form malachite and azurite, precipitated along fractures within the sericite-quartz altered magmatic rocks and calcite-bearing carbonate rocks. The B-Kafa mineralisation, regarded as a continuation of the hydrothermal system that formed the A-Kafa orebody (Yılmazer *et al.*, 2003), is mainly hosted by intensely brecciated limestones, and is juxtaposed with the Na-Ca and K-Fe alteration of A-Kafa along the ENE-WSW trending faulting (Figs. 5).

Constraints on Fluid Source

$^{40}Ar/^{39}Ar$ dating of the Murmano pluton and associated K-Fe alteration (*ca*. 77 to 73 Ma), showed that the timing of magmatism and K-Fe alteration overlaps. This association between the magnetite mineralisation and potassic alteration suggests that K-Fe alteration and Fe mineralisation are temporally and spatially related to the emplacement, crystallisation and cooling of the Murmano pluton at Divriği. The $\delta^{34}S_{VCDT}$ sulphur isotope composition of late pyrite of between 11.5 and 17.4‰ (Marschik *et al.*, 2008) favours a non-magmatic sulphur source of probable evaporitic origin, as suggested by Marschik *et al.* (2008). Similarly, calcite from the Divriği deposit has values of $\delta^{18}O_{VSMOV}$ between 15.1 and 26.5‰ and $\delta^{13}C_{VPDB}$ between −2.5 and 2.0‰ (Marschik *et al.*, 2008), which are compatible with an involvement of modified marine evaporitic fluids during the post-magnetite, late hydrothermal stages. However, as the calcite and pyrite are products of late alteration, overprinting the main magnetite mineralisation and earlier Na-Ca and K-Fe stages, these isotope values may only relate to the fluids that produced that alteration, and any inference on their bearing on the genesis and origin of fluids that formed the earlier (relatively high temperature) Na-Ca and K-Fe alteration is debatable. However, the temporal and spatial overlap between the magmatism and alteration, and the common development of alteration and mineralisation within the magmatic rocks, favour the interpretation that the fluids are related to the emplacement and crystallisation of calc-alkaline to alkaline magma intruding the ophiolites and ophiolitic mélange. Although, there is no equivocal evidence for the source of Na and Cl in the Divriği area, these elements may have been contributed by the marine water trapped by the fractures and pore spaces within the ophiolitic mélange and carbonate rocks.

Hasançelebi-Karakuz IOCG Mineralisation

Local Geology

The Hasançelebi iron oxide deposit, with calculated reserves of 94.8 Mt at 23% Fe_3O_4 (Yuce *et al*., 2005), and around 0.8 to 2.75% Cu, 1.9% Ni, 0.04 to 2 g/t Au (Ay *et al*., 2005), is located approximately 80 km northwest of Malatya, in eastern Turkey (Fig. 7). The host sequence (Figs. 7a and b) comprises an extension-related volcanic-volcanoclastic sequence, intruded by syenitic rocks, within the Hekimhan basin, formed after the emplacement of northerly-derived ophiolitic nappes over the Tauride-Anatolide platform during the uppermost Cretaceous (Kuşcu *et al.*, 2007a, b; 2008).

The underlying ophiolitic rocks of the Hocalikova ophiolites and epi-ophiolitic sequences below the basin (Gürer, 1992), are chaotic units in the southern parts of the district. They comprise gabbro-diorite, serpentinised pyroxenite, harzburgite and lherzolite, and are juxtaposed with scapolitised syenitic and trachytic rocks across an east-west trending strike-slip fault (Figs. 7b), which has a south verging, 60 to 70° reverse component. The overlying Hekimhan formation contains coarse continental clastic rocks at the base, grading upwards into shallow marine sandstone-marl-shale interbeds at the top (Gürer, 1992; 1996). The volcanics-volcanoclastic rocks of the Hasançelebi volcanics are either intercalated with the fine-grained facies of the Hekimhan formation, or occur as dykes cutting through the basin infill. These volcanic rocks include dolerite, trachytic, spilitic basalt, pillow basalt and pyroclastic rocks. All of these units were intruded by the Yucesafak syenite, which comprises syenite-syenodiorite, late syenite porphyry and microsyenite porphyry, and by dolerite occurring mostly as vertical, east-west trending dykes or as sill-like intrusions cutting both the Hekimhan formation and Hasançelebi volcanics. The unconformably overlying Middle to Late Eocene (Gurer, 1992) Akpinar formation consists primarily of sedimentary and volcanic rocks (Leylekdağ volcanics; Gurer, 1992). The sedimentary component of this latter sequence includes a basal conglomerate and sandstone interlayer, which grades upwards into shale to marl. These sediments are overlain by dacitic tuffs to agglomerates and are intruded by predominantly dacite and rhyodacite. They are in turn unconformably overlain by the Mio-Pliocene sedimentary rocks of the Agabayir conglomerate, and volcaniclastic to volcanic rocks of the Yamadag volcanics. The Yamadag volcanics comprise agglomerates at the base, grading upward into tuff-bearing sequences. All of these clastic to volcaniclastic rocks are overlain by a thick pile of basalt to rhyolite flows that can be traced for several tens of kilometres to the east and north.

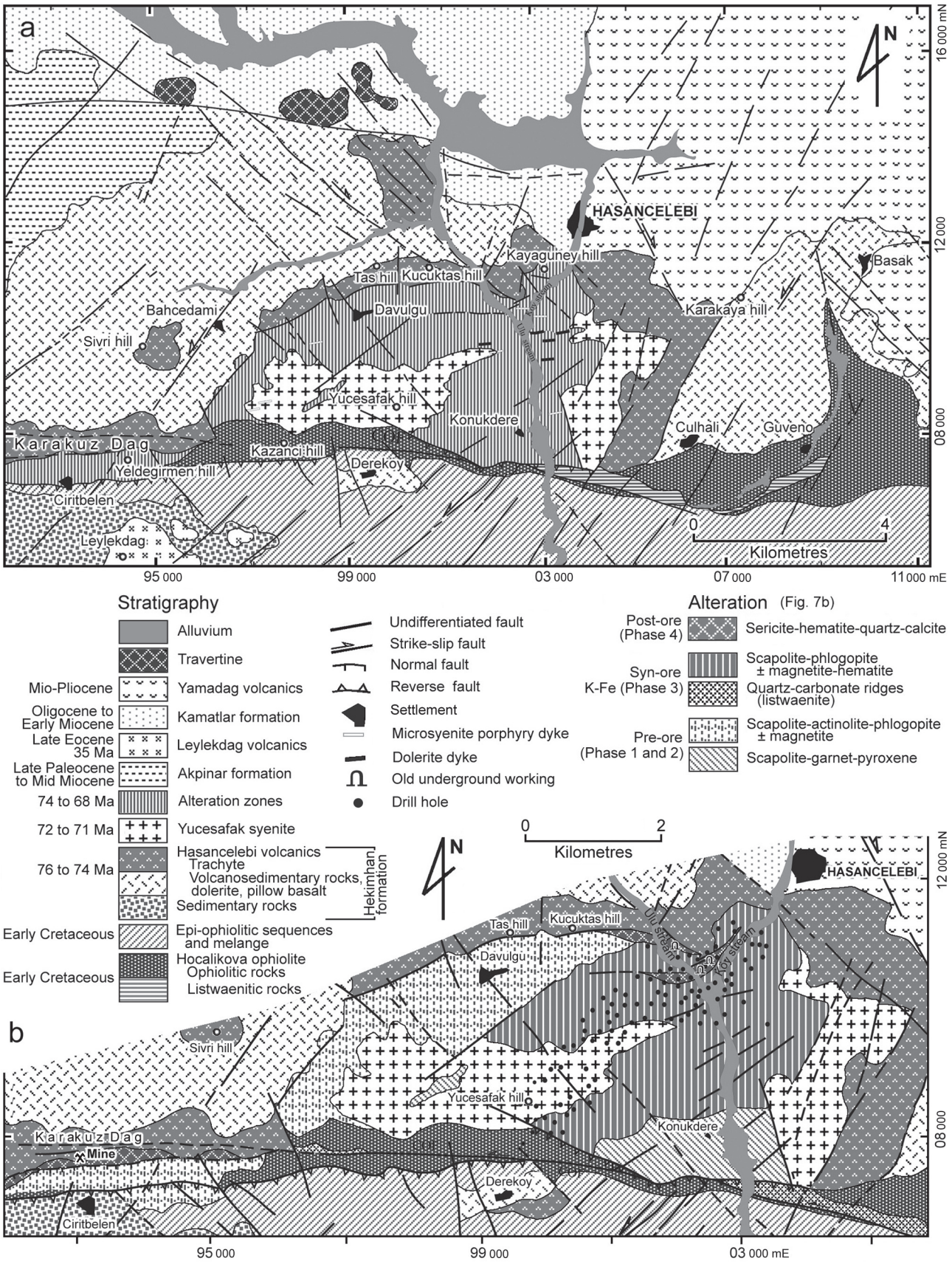

Figure 7: Geological setting of the Hasançelebi deposit **(a)** simplified geological map showing the main rock types and the undifferentiated alteration zone, and **(b)** geological and alteration map of the mineralised area, showing the individual alteration styles (Modified from Kuşcu, *et al.*, 2007c)

Geochemistry of Magmatic Rocks

In general, the Hasançelebi volcanics and Yucesafak syenite have alkaline characteristics, and are classified as basalt, trachyte, trachy-andesite, trachy-basalt, syenite and syenodiorite (Figs. 8a and b). The rocks are generally enriched in REE relative to chondrites (Fig. 8c) and in LFS compared to HFS elements (Fig. 8d). Prominent negative anomalies are recorded in K, Ti, Ba and Nb (Table 4), and slight positive anomalies in Rb and Th. All samples are characterised by significant flattening of HREE relative to the LREE, and a marked depletion in Eu in syenitic and trachytic rocks (Figs. 8c and d). The syenitic rocks are more enriched in HREE compared to trachytic and doleritic rocks. Nb, Y, Yb and Ta values suggest WPG (within-plate granite), VAG (volcanic arc granite) and syn-COLG (collisional granite) settings (Figs. 8e and f). The Th/Yb vs Ta/Yb plot (Fig. 8g) suggests the derivation of magmatic rocks from a mantle source, which was either previously enriched by small-degree partial melts (displacement along the mantle array), and/or metasomatised by ancient subduction. The displacement of all samples away from a mantle array towards a higher Th/Yb ratio in Fig. 8g is likely to support enrichment by an older subduction event. However, the

Table 4: Representative geochemical analyses of selected samples from magmatic rocks in the Hasançelebi region. nd = not detected.

	Syenitic rocks						**Trachytic rocks**			**Dolerite**				
Sample	318	320	321	326	Y-43	Y-2	Y45	331	H3	323	325	Y-11	Y-23	Y-41
SiO_2	58.10	56.66	61.15	59.23	60.17	67.23	59.44	45.64	62.47	47.17	54.59	45.51	42.26	55.18
Al_2O_3	16.24	16.36	15.44	15.45	15.05	14.18	16.11	16.20	17.74	15.34	15.93	16.37	17.09	14.87
Fe_2O_3	3.90	2.40	1.48	1.35	1.43	1.51	7.02	11.32	1.35	7.02	13.65	10.18	8.26	2.51
CaO	4.98	5.49	5.08	7.58	7.81	4.28	0.46	7.49	2.12	11.49	4.19	11.19	7.87	7.46
MgO	2.33	3.78	1.44	0.15	0.11	0.10	0.05	6.26	1.33	4.80	2.70	6.22	6.10	4.70
Na_2O	3.40	8.24	2.90	8.50	8.42	8.07	0.51	4.69	5.43	4.97	5.17	1.33	3.27	7.13
K_2O	6.94	1.29	8.23	0.40	0.13	0.14	13.30	2.78	6.37	1.65	3.46	3.74	4.87	1.11
TiO_2	1.32	0.45	1.07	0.52	0.45	0.50	0.30	1.07	0.63	1.83	1.99	1.50	0.77	1.33
MnO	0.03	0.04	0.04	0.05	0.05	0.04	0.11	0.04	0.03	0.08	0.11	0.06	0.07	0.05
P_2O_5	0.36	0.20	0.29	0.12	0.11	0.18	0.10	0.42	0.03	0.47	0.60	0.39	0.47	0.04
LOI	2.00	5.05	2.29	5.87	5.94	3.48	1.80	3.65	1.92	4.45	1.68	3.89	8.85	5.36
TOTAL	99.95	99.95	99.32	99.23	99.67	99.70	99.16	99.43	99.42	99.22	99.57	99.98	99.89	99.74
Ba	2940	271	3598	122	74	429	69	605	4590	1219	1045	962	2240	1160
Rb	100	19	49	4	0	0	266	144	89	64	105	137	131	17
Sr	326	234	273	175	161	72	113	439	400	573	242	414	96	242
Cs	2.34	1.75	0.29	0.13	0.00	0.50	1.00	5.55		0.98	1.71	0.90	6.60	2.20
Li	326.00	16.40	15.80	23.80	0.00	0.00	0.00	35.00	0.00	48.00		0.00	0.00	0.00
Ga	21	21	24	27	23	22	15	18	23	19	21	16	27	18
Ta	2.50	3.40	2.86	6.30	2.80	2.50	14.00	1.24	4.80	1.86	2.30	1.00	1.90	3.40
Nb	40.80	45.00	44.00	98.00	44.00	32.00	35.00	17.10	73.00	25.60	34.70	16.00	92.00	66.00
Hf	8.90	8.20	8.80	17.30	9.40	7.20	2.80	4.54	8.60	3.60	6.70	4.00	3.80	9.90
Zr	341	370	421	945	413	283	302	187	431	159	256	151	125	420
Tl	1	nd	1	nd	nd	nd	nd	1	nd	1	1	1	nd	1
Y	44.3	23.0	35.0	42.0	39.0	28.0	25.0	16.3	43.0	23.0	42.3	25.0	94.0	71.0
Th	20.40	36.00	23.90	62.00	23.10	24.20	12.30	14.40	26.30	6.28	16.35	9.70	31.30	21.90
U	13.05	8.40	11.86	12.30	10.00	5.50	0.00	7.30	8.00	5.44	6.39	4.10	27.70	9.70
Cr	30.0	3.0	6.3	2.1	177.0	233.0	150.0	178.0	186.0	908.0	10.0	169.0	51.0	71.0
Ni	38	23	10	23	20	20	20	69	26	31	8	48	979	0
Co	9.6	6.0	6.3	6.7	2.0	1.0	9.0	29.7	4.0	12.6	14.8	16.0	167.0	4.0
Sc	38.0	4.5	8.5	2.1	5.0	7.0	0.0	25.0	3.0	24.0		23.0		8.0
V	113.0	35.0	42.4	23.8	26.0	33.0	16.0	209.0	18.0	214.0	175.0	158.0	299.0	35.0
Pb	14.0	2.2	9.1	2.1	5.0	5.0	231.0	3.5	nd	4.2	10.0		15.0	5.0
Zn	45.0	22.0	7.8	1.6	30.0	30.0	30.0	35.9	nd	19.3	73.0	32.0	96.0	30.0
Sn	7.0	5.5	4.9	5.1	4.0	3.0	3.0	0.7	5.0	2.1	3.0	3.0	1.0	8.0
La	70.2	30.0	88.0	31.0	19.6	19.9	506.3	41.0	31.4	50.0	56.1	32.3	92.0	76.9
Ce	145.5	67.3	172.0	80.0	53.0	40.8	11.4	76.0	89.7	79.0	109.5	59.1	141.0	177.0
Pr	15.6	8.1	14.4	10.8	7.6	4.8	37.1	7.4	12.1	6.5	12.6	7.1	24.2	20.8
Nd	52.5	31.6	49.0	45.0	30.9	17.8	5.7	29.2	45.0	23.3	46.6	27.7	112.0	72.2
Sm	9.2	5.5	8.1	9.0	6.9	3.7	1.1	4.8	8.7	4.3	9.3	5.5	27.7	13.1
Eu	2.6	0.8	2.5	1.2	1.3	0.7	4.3	1.2	2.2	1.2	3.3	2.7	8.6	3.3
Gd	9.0	4.5	6.6	7.4	6.1	3.7	0.6	2.9	8.0	4.4	9.6	4.8	24.3	11.5
Tb	1.3	0.6	1.0	1.2	1.0	0.6	3.7	0.5	1.3	0.6	1.4	0.8	3.6	1.9
Dy	7.2	4.0	6.2	8.2	6.0	3.9	0.8	3.0	6.9	3.9	7.8	4.2	17.6	10.7
Ho	1.5	0.8	1.3	1.6	1.2	0.8	2.6	0.6	1.5	0.8	1.6	0.8	3.2	2.1
Er	4.5	2.3	3.7	4.9	3.8	2.5	0.5	1.7	4.4	2.4	4.7	2.4	8.9	6.4
Tm	0.6	0.3	0.5	0.7	0.6	0.4	3.0	0.2	0.7	0.3	0.7	0.3	1.3	0.9
Yb	4.4	2.4	3.7	4.8	3.8	2.6	0.5	1.6	4.5	2.3	4.3	2.0	7.7	6.0
Lu	0.6	0.4	0.6	0.7	0.6	0.4	6.6	0.2	0.6	0.4	0.7	0.3	1.1	0.9

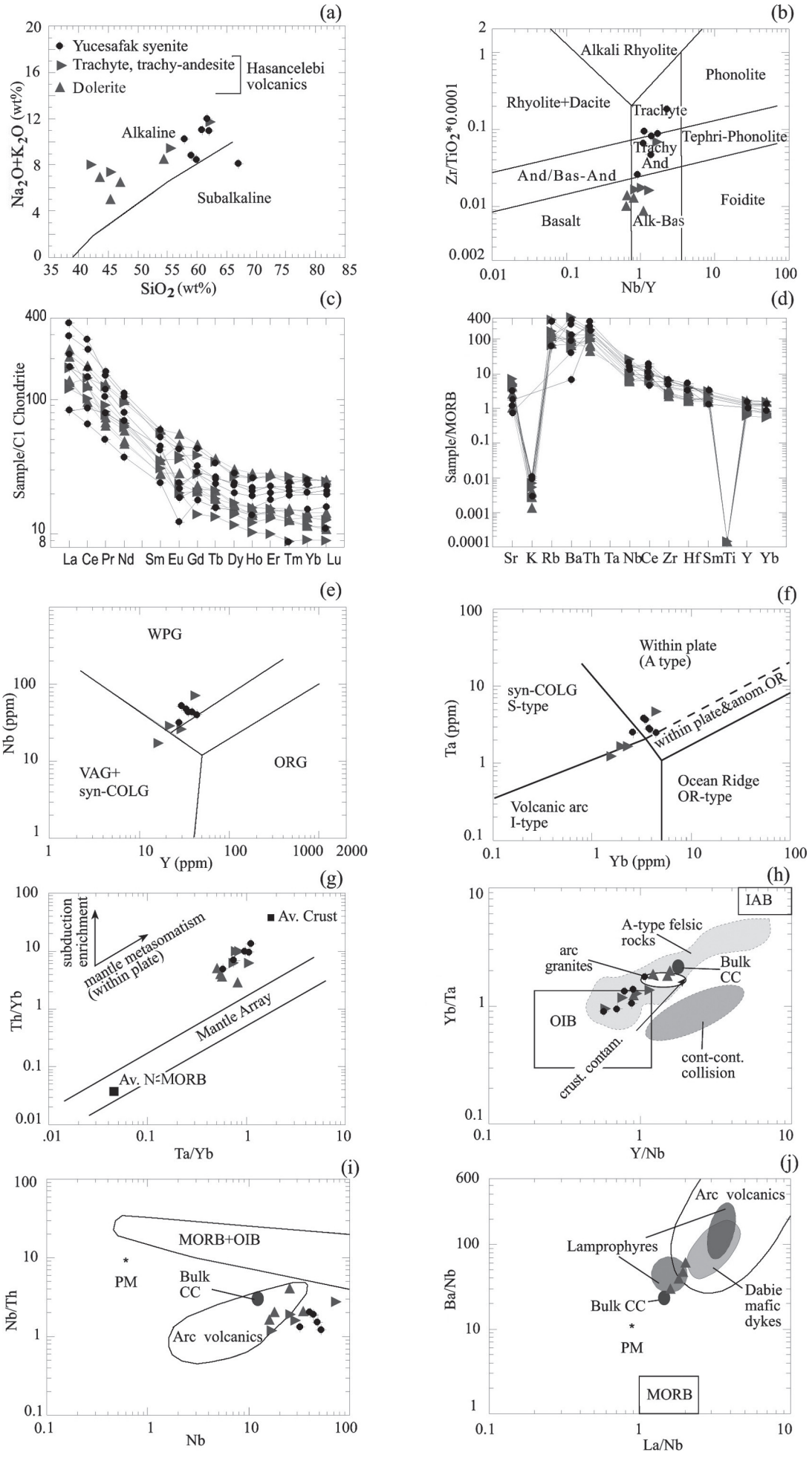
(a)
Yucesafak syenite
Trachyte, trachy-andesite
Dolerite
Hasancelebi volcanics
Alkaline
Subalkaline
Na2O+K2O (wt%)
SiO2 (wt%)
(b)
Alkali Rhyolite
Phonolite
Rhyolite+Dacite
Trachyte
Tephri-Phonolite
Trachy And
And/Bas-And
Foidite
Basalt
Alk-Bas
Zr/TiO2*0.0001
Nb/Y
(c)
Sample/C1 Chondrite
La Ce Pr Nd Sm Eu Gd Tb Dy Ho Er Tm Yb Lu
(d)
Sample/MORB
Sr K Rb BaTh Ta NbCe Zr Hf SmTi Y Yb
(e)
WPG
VAG+ syn-COLG
ORG
Nb (ppm)
Y (ppm)
(f)
Within plate (A type)
syn-COLG S-type
within plate&anom.OR
Ocean Ridge OR-type
Volcanic arc I-type
Ta (ppm)
Yb (ppm)
(g)
subduction enrichment
mantle metasomatism (within plate)
Av. Crust
Mantle Array
Av. N-MORB
Th/Yb
Ta/Yb
(h)
IAB
A-type felsic rocks
arc granites
Bulk CC
OIB
cont-cont. collision
crust. contam.
Yb/Ta
Y/Nb
(i)
MORB+OIB
PM
Bulk CC
Arc volcanics
Nb/Th
Nb
(j)
Arc volcanics
Lamprophyres
Bulk CC
Dabie mafic dykes
PM
MORB
Ba/Nb
La/Nb

enrichment of magmatic rocks in both LREE and HREE (Fig. 8c) further suggests that metasomatism in the mantle may not be solely due to subduction. In addition, the trend yielded by the data points in Fig. 8h, implies superimposed crustal contamination, probably accompanied by fractional crystallisation. The enrichment by an earlier subduction or by crustal contamination can be best observed on combined Yb/Ta vs Y/Nb (Whalen *et al.*, 1987; Best and Christiansen, 2001) and Nb/Th vs Nb plots (Figs. 8h, i and j). Almost all samples plot in the OIB (ocean island basalt) and arc granite fields as a linear trend, defining crustal contamination of a mantle-derived basaltic melt (Figs. 8i and j). The melt source is likely to be lithospheric mantle, based on La/Nb ratios of greater than 1.0 (De Paolo and Daley, 2000) (Fig. 8j). However, the samples all plot in the subfield of the Jurassic White Mountain A-type granitoids consisting mainly of syenitic, granitic and mafic rocks generated in an extension-related setting (Fig. 8h; Best and Christiansen, 2001). Such magmas resulted from partial melting under an extension-dominated regime, following subduction. The extension in eastern-southeastern Anatolia is attributed to the roll-back of the subducting slab, coupled with orogen-parallel initial extension-exhumation on the overriding plate. This followed emplacement of the northerly-derived ophiolite (of the Vardar ocean) which was obducted during the closure of the NeoTethyan ocean along the Bitlis-Zagros subduction zone (Kuşcu *et al.*, 2007a, b, c, d).

Geochronology

U-Pb and ^{40}Ar-^{39}Ar geochronology of igneous rocks returned ages for trachyte and dolerite of 76.84 Ma and 74.40 Ma, respectively, and 71.30 Ma for syenite (Table 3). The dacites in the Leylekdağ volcanics gave an ^{40}Ar-^{39}Ar age of 34.4 Ma (Kuşcu *et al.*, 2007c, d). ^{40}Ar-^{39}Ar hornblende and biotite geochronology for dolerite intrusion yielded ages of 74.40±0.51 and 74.26±0.45 Ma, respectively, while ^{40}Ar-^{39}Ar determinations on hydrothermal biotite from an altered dolerite dyke gave an age of 74.32±0.42 Ma. Two samples of brown hydrothermal biotite from Hasançelebi also yielded plateau ages of 73.43±0.41 Ma and 74.92±0.39 to 73.12±0.75 Ma (Table 3; Marschik, *et al.*, 2008). Hydrothermal biotite age, which remains within the age range of dolerite intrusion (Table 3; Kuşcu *et al.*, 2007c; 2008), shows that pre-ore K-Fe alteration is temporally related to the emplacement of dolerite dykes. ^{40}Ar-^{39}Ar K feldspar dating of syn-ore K-Fe alteration and associated magnetite mineralisation, yielded ages ranging from 70.48±0.42 to 68.64±0.42 Ma (Table 3). A comparison of the crystallisation age of syenite and microsyenite porphyry dykes, suggests a temporal association between syenitic magmatism, and syn-ore K-Fe alteration and iron oxide mineralisation at the Hasançelebi deposit. A genetic link between the alteration and trachytic magmatism is unlikely, because the trachyte, trachy-andesite-type rocks (76.84±0.67 Ma) are older than the alteration assemblages formed during both phases.

Figure 8 (facing page): Geochemical classification and discrimination diagrams for igneous rock within the Hasançelebi deposit: **(a)** Total alkalis versus silica (TAS) plot of Irvine and Baragar (1971); **(b)** Modified Zr/TiO_2-Nb/Y plot (Pearce, 1996) of Winchester and Floyd (1977); **(c)** Rock/chondrite-normalised REE; **(d)** rock/MORB-normalised spidergrams; **(e)** Nb-Y and **(f)** Ta-Yb diagrams of Pearce, *et al.*, (1984); **(g)** Th/Yb vs Ta/Yb diagram (Pearce, 1983) showing the effect of mantle metasomatism; **(h)** Yb/Ta-Y/Nb diagram (Best and Christiansen, 2001; Whalen, *et al.*, 1987) diagram showing the effect of crustal contamination and within-plate signature; **(i)** Nb/Th-Nb diagram (arc volcanics, OIB, continental crust, primitive mantle data are after Schimidberger and Hegner (1999); and **(j)**Ba/Nb-La/Nb diagram (Jahn, *et al.*, 1999).

Alteration

Drill hole data reveals the Hasançelebi deposit occurs mainly as sub-horizontal to horizontal lenses and "pocket-like" iron oxide bodies composed chiefly of magnetite, that has often been converted to hematite. Uneconomic copper mineralisation is present as either chalcopyrite disseminations within sericite-quartz±calcite veins, or as malachite-goethite stained veinlets accompanied by gold.

The iron oxide mineralisation within the Hasançelebi district is accompanied by pervasive Na-Ca alteration (mainly scapolite-garnet-diopside, scapolite-actinolite) overprinted by K-Fe alteration (mainly phlogopite with minor K-feldspar). The copper-gold±hematite mineralisation is mainly hosted by sericitised rocks containing veins of sericite-quartz-calcite. Field work, supplemented by detailed alteration petrography, shows that the hydrothermal evolution of the Hasançelebi district broadly resulted from two discrete intrusive events: (1) early dolerite invading the trachytic and sedimentary-volcanosedimentary rocks, and (2) late syenite, microsyenite porphyry intrusions into the entire Hekimhan basin. The first event resulted in pre-magnetite alteration, characterised by sodic (early Na) and potassic (early K) alteration assemblages restricted to intrusive contacts between dolerite and trachytic rocks with or without disseminated fine-grained magnetite (Kuşcu *et al.*, 2008). The second intrusive event resulted in pre-magnetite sodic-calcic (late Na-Ca) and syn-magnetite potassic (late K-Fe) alteration. Both are overprinted by post-magnetite sericitisation (sericite, early-quartz, barite, early-calcite, fluorite) and copper-gold mineralisation, and by late alteration (late-calcite, late-quartz, barite, goethite, azurite and malachite).

Early, pre-magnetite sodic alteration resulted in the generation of fine-grained scapolite and phlogopite (early scapolite and early phlogopite). The late Na-Ca and syn-magnetite K-Fe alteration phases are more pervasive, regional and coarse grained. The pre-magnetite alteration minerals are preserved as relicts replaced or enclosed by assemblages produced by the syn-ore alteration.

The pre-magnetite, late Na-Ca alteration consists of: (1)scapolite-garnet-diopside, titanite and apatite, which mainly occurs in association with syenitic rocks, and (2) scapolite-actinolite that is the dominant assemblage accompanying trachytic rocks. On a regional scale, syn-magnetite late K-Fe alteration (phlogopite±K feldspar) and magnetite, typically post-date the pre-magnetite early Na and late Na-Ca alteration. Petrographic and field observations demonstrate that syn-ore phlogopite occurs as veins and veinlets within the scapolite-rich rocks. The main magnetite-hematite mineralisation is hosted by trachytic (Fig. 7b) and syenitic rocks that contain syn-ore phlogopite±actinolite-epidote.

The sericitic alteration is post-magnetite, and is largely characterised by an assemblage of sericite, early quartz, ±early calcite, barite and fluorite, which overprinted phlogopite±scapolite±actinolite-bearing rocks as veins or as replacements, and is associated with hematite development (Kuşcu *et al.*, 2007c). Hematite and copper-gold±hematite mineralisation is spatially associated with sericite-carbonate-epidote and quartz-bearing assemblages of this alteration phase, superimposed upon phlogopite-

magnetite and scapolite-actinolite alteration within trachytic rocks. This mineralisation is predominantly found replacing the main magnetite orebody along shear zones. The copper mineralisation occurs as chalcopyrite-quartz veins and veinlets, oxidised to produce malachite-goethite staining. Copper and gold grades are up to 2.7% and 2 g/t, respectively (Ay *et al.*, 2005). Late overprinting alteration, produced vein-like replacement of late calcite, pyrite, ankerite and barite, and goethite-malachite (Figs. 4k and l) throughout the magnetite-hematite bodies and sericitised rocks (Kuşcu *et al*., 2007c; 2008).

Constraints on the Fluid Source

Stable isotope analyses for O and H were carried out on pre-ore K-Fe alteration early phlogopite, and post-ore alteration sericite (Table 5; Kuşcu *et al.*, 2008). Phlogopite, sericite, barite, early-calcite, fluorite and early-quartz gave $\delta^{18}O_{mineral}$ values of 9.46‰, 8.87‰, 10.14‰, 12.8‰, 8.53‰ and 15.13‰, respectively (Table 5). The $\delta D_{mineral}$ of phlogopite, sericite, barite, early calcite, fluorite and early quartz yielded -89.54‰, -107.21‰, -85.65‰, -122.28‰, -95,16‰ and -124‰, respectively. Phlogopite-H_2O, muscovite/sericite-H_2O, quartz-H_2O (Zheng 1993a), calcite-H_2O (Zheng 1993b) and barite-H_2O (Kusakabe and Robinson, 1977) fractionations were used to calculate the isotopic composition of coexisting water using the average temperatures obtained from fluid inclusions for each alteration stage (Sezerer-Kuru *et al*., 2006). The fractionation factors for early-calcite and phlogopite (Bowers and Taylor, 1985), sericite and barite (Suzuoki and Epstein, 1976) and quartz (Zheng, 1993a and Clayton *et al.*, 1972) were used to calculate δD_{H_2O} values. The $\delta^{18}O_{H_2O}$ and δD_{H_2O} results are shown in Table 5. The isotope composition of the fluid calculated from the mineral-water pairs (Table 5) indicates a fluid of dominantly magmatic origin. The $\delta^{18}O$ and δD values of fluids that produced K-Fe alteration and sericitisation partially overlap the characteristic range for traditional magmatic waters (Taylor, 1986). Except for calcite-I, all minerals remain in the range of the primary magmatic water field.

The regional geological data also put constraints on any non-magmatic evaporitic-brine model, in that there are no evaporitic units and/or sedimentation of Late Cretaceous age within the Hekimhan basin. The known evaporitic rocks unconformably overly the host sequence containing the alteration and mineralisation within the district. Therefore, the stable isotope and geochronology data have important implications for the genesis of the Hasançelebi IOCG mineralisation, indicating the fluids that produced the Na, Na-Ca and K-Fe alteration during both phases were largely magmatic, or at least have a genetic connection with the magmatism in the district. However, an admixture of magmatic and non-magmatic fluids may also be plausible, while there could have been an introduction of external fluids (e.g., seawater or basinal brines) during sericitisation and late alteration (Kuşcu *et al.*, 2007c; 2008).

Structural Controls

The alteration and iron-(copper-gold) mineralisation of the Hasançelebi district is localised within east-west-, ENE-WSW- to northeast-southwest-trending structures (Kuşcu *et al.*, 2007c). For the most part, the pre-magnetite alteration assemblage (early-sodic and potassic) is largely distributed along east-west trending structures (Figs. 7a and b), which are also the loci for emplacement of dolerite dykes within the district. On the other hand, the assemblage at syn-magnetite alteration (late-potassic) is largely preserved as pervasive and massive replacement features focused along 60 to 70º (ENE-WSW)-trending factures. These are conformable with the general trend of first phase deformation (D_1) structures (Kaymakci *et al.*, 2006), indicating that magmatism and alteration were intermittently active over a protracted series of tectonic and hydrothermal events, mainly during the Late Cretaceous (Kaymakci *et al.*, 2006; Kuşcu *et al.*, 2007c).

Iron oxide-(Cu±Au) Mineralisation in the WAEP

The WAEP (Western Anatolian Extensional Province) hosts several porphyry copper-gold, gold or copper-molybdenum, and high- to low-sulphidation epithermal gold, gold-silver vein-type deposits, as well as occurrences of skarn iron-copper, copper and IOCG-style mineralisation. Most are located within the Biga (Canakkale) and Balıkesir regions (Fig. 4) where continuous intrusive and extrusive magmatism is recorded from the Eocene to Pliocene. The porphyry and epithermal deposits in the WAEP have spatial and temporal associations with Eocene-Oligocene intrusive and extrusive magmatic rocks from Early to Middle Miocene, and even to Late Miocene, and have characteristics similar to those in the U.S. Cordillera and Rhodope-Serbo-Macedonian regions. Published K-Ar geochronology indicates that there are four main pulses of magmatism and associated hydrothermal activity in western Anatolia. The skarn and gold, copper-molybdenum porphyry deposits are the result of three significant magmatic pulses that took place between Early Campanian to Early Maastrichtian (Late Cretaceous), Early Eocene to Middle Oligocene(?) and Late Oligocene to Middle Miocene. The

Table 5: Hydrogen and oxygen isotope analyses (per mil) and calculated isotope composition of fluid at the Hasançelebi deposit. n.c = no calculation

Mineral	$\delta^{18}O_{mineral}$ ‰	$\delta D_{mineral}$ ‰	T_h°C [6]	$\delta^{18}O_{H_2O}$ ‰	δD_{H_2O} ‰
Sericite	8.87	-107.21	320-390	7.79-8.78 [1]	-79.71,-89.21 [5]
Phlogopite	9.46	-89.54	700	5.61 [1]	-80.54 [4]
Fluorite	8.53	-95.16	210-280	n.c	n.c
Barite	10.14	-85.65	190-380	9.25-3.13 [3]	-85.65 [5]
Calcite-I	12.80	-122.28	180-320	7.78-2.15 [2]	-122.28 [4]
Quartz-I	15.13	-124.00	290-370	6.59-7.87 [2]	n.c

[1] $\delta^{18}O_{H_2O}$ values were calculated according to Zheng (1993a)
[2] $\delta^{18}O_{H_2O}$ values were calculated according to Clayton *et al.* (1972)
[3] $\delta^{18}O_{H_2O}$ values were calculated according to Kusakabe and Robinson (1977)
[4] δD_{H_2O} values were calculated according to Bowers and Taylor (1985)
[5] δD_{H_2O} values were calculated using experimentally determined equilibrium hydrogen isotope fractionation factors by Suzuoki and Epstein (1976)
[6] Homogenization temperatures are from Kuru *et al.* (2006)

high- and low-sulphidation-type epithermal and iron-copper skarn deposits, and the IOCG-style mineralisation appear to be associated with the third pulse. This phase resulted from core-complex or slab-pull to roll-back extensional mechanisms (Okay and Satır, 2000; Innocenti *et al.*, 2005) that occurred between the Late Oligocene to Middle Miocene and Middle to Late Miocene, respectively. The major porphyry Au, Au-Mo deposits are associated with, or are hosted by extrusive alkaline magmatism of Middle(?) to Late Miocene to Mio-Pliocene age. Although there are several examples of iron-oxide mineralisation with anomalous Cu enrichment, only the Şamlı deposit best fits into the IOCG class. The Şamlı (Balıkesir) iron oxide-copper-(gold) mineralisation is located within the Sakarya zone that was formed during the closure of the PalaeoTethys ocean (Tekeli, 1981; Şengör *et al.*, 1984; Okay *et al.*, 1990; Akyüz and Okay, 1996; Okay and Göncüoğlu, 2004).

Şamlı IOCG Deposit

The Şamlı iron oxide deposit is located 25 km to the northeast of Balikesir and covers an area of almost 30 km^2, including the mineralisation on the Bakırlık ("copper hill"), Kocaçal, Menekşe and Kaletepe hills. The existence of recognised and potential iron oxide-copper-(±gold) mineralisation in the WAEP has only recently been defined (Kuşcu *et al.*, 2005b). The mining history of the Şamlı iron oxide deposits dates back to Byzantine times, when both iron and copper were reportedly exploited. Since the 1950`s, the open pit at Bakırlık Hill has been intermittently mined for iron ore. The calculated reserve at Bakırlık Hill is 96 000 tonnes with an average grade of 50 to 53% Fe (MTA, 1964), while the copper content in the open pit area averages more than 1% (locally as high as 6.78% and 7.74% Cu; Leo and Genc, 1986). This is what remains after the historical mining and open pit production since 1950. Gold and silver contents range from 5 to 8 ppm, and 23.8 to 66.9 ppm, respectively (Erkan Yılmazer, unpublished data). Almost all available cobalt assays are high, ranging up to 300 ppm.

Local Geology

The host rocks at Şamlı comprise the Triassic Karakaya Complex and the Tertiary Şamlı pluton (Figs. 9a and b), which are unconformably overlain by Neogene cover units (Fig. 9). The Karakaya Complex is a volcanic-volcanosedimentary sequence, consisting predominantly of pyroclastics and tuffs that alternate with carbonates and turbiditic greywackes, but also contains Permian to Carboniferous olistoliths of spilitic basalt and dolerite. These rocks underwent low-grade regional metamorphism during the latest Triassic (Akyürek and Soysal, 1983; Koçyiğit, 1987; Okay *et al.*, 2000). Within the deposit site (open pit area), the Karakaya Complex consists mainly of metapelitic rocks, metadolerite and recrystallised limestone.

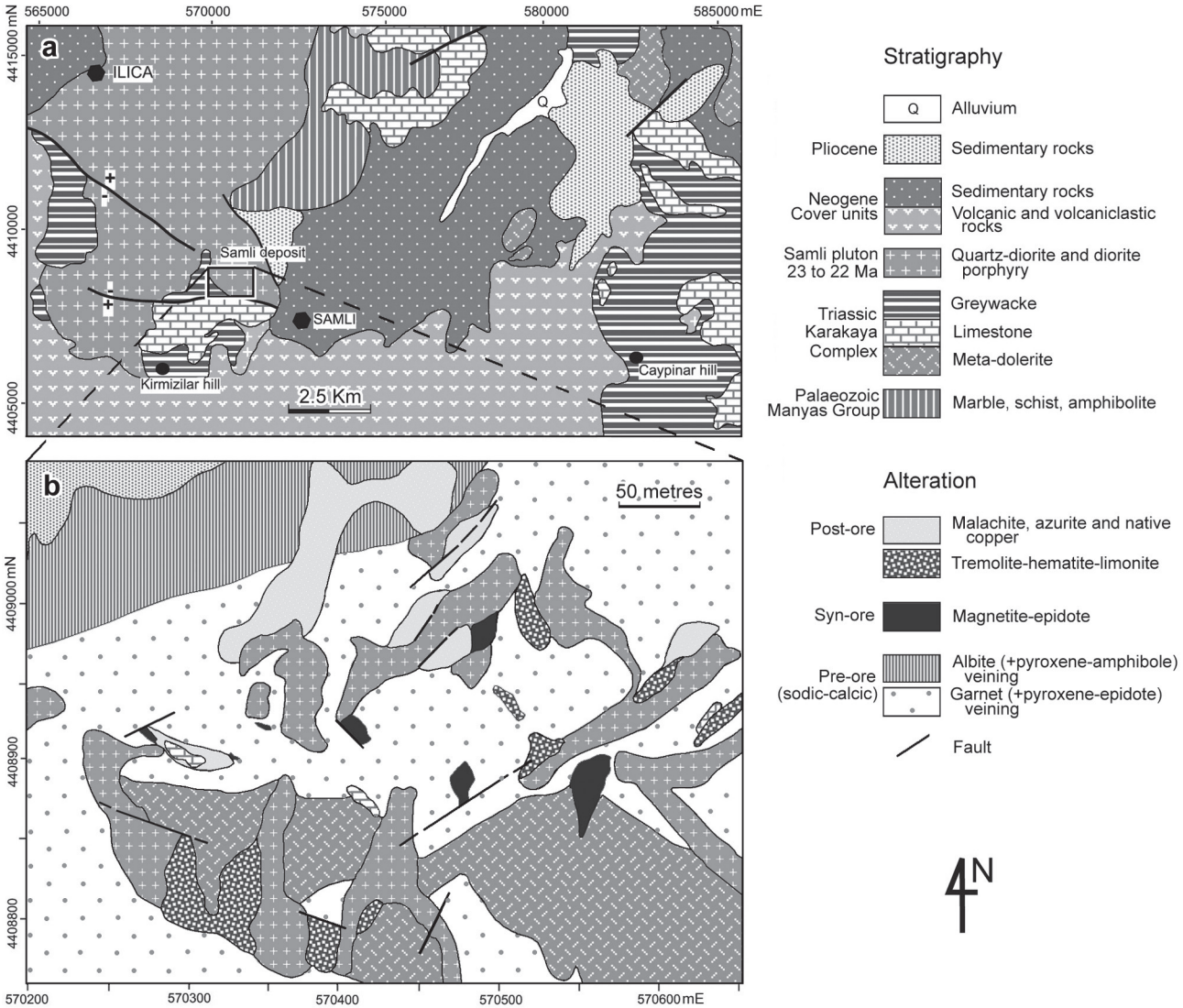

Figure 9: (a) Simplified geological map of the Şamlı district, **(b)** alteration map of the Şamlı open pit area shown as a frame on (a); revised from Erkan Yilmazer unpublished thesis data, and Kuscu *et al.*, 2005.

Metadolerite, as defined previously (Yurt and Yurt, 1981; Leo and Genç, 1986), herein refers to dense, black aphanitic rocks, typically consisting of plagioclase laths, pale secondary hornblende and disseminated magnetite. The metadolerite and recrystallised limestone occur either as blocks within the Karakaya Complex, or as roof-pendants within the Şamlı pluton (Figs. 9b). The Neogene cover succession is composed of volcanic breccia, massive lava, rare tuff and volcanogenic clay, and can be correlated with the Ezine volcanics of Akyüz and Okay (1996). The Neogene cover unit also includes coarse clastics, conglomerate, sandstone, shale, marl and volcanics (Leo and Genç, 1986; Okay *et al.*, 1990).

The Şamlı pluton is a large, intermediate to mafic intrusive body emplaced into the recrystallised limestone and metadolerite of the Karakaya Complex (Fig. 9). The overall composition of the pluton, including associated tabular bodies and isolated masses, ranges from granite porphyry, to quartz diorite, diorite porphyry, and granodiorite to syenite (Leo and Genc, 1986). The main plutonic mass in the immediate deposit area is composed dominantly of granodiorite to quartz diorite and diorite porphyry. The diorite porphyry and quartz diorite occur as dykes and plugs of mafic end-members of a magma formed by mixing/mingling of mafic and felsic magmas. The granite porphyry appears to be relatively late in the magmatic sequence, and intrudes into the diorite and diorite porphyry. Thin (3 to 5 cm) aplite dykes, which are not exposed at the deposit site, post-date the alteration and granite porphyry. Sodic-calcic alteration and iron-copper mineralisation is most likely related to the emplacement of granite porphyry to granodiorite plugs and dykes into the quartz diorite and diorite porphyry and the Karakaya Complex. Gunalay (1968) reported that the term "syenite" has been applied to pervasively metasomatised diorite that resulted from alteration.

Geochemistry of Magmatic Rocks

The magmatic rocks associated with iron oxide-copper mineralisation at Şamlı are classified as sub-alkaline, with calc-alkaline to calcic characteristics (Figs. 10a and b). They are metaluminous to peraluminous, and have compositions of granodiorite, quartz diorite, diorite porphyry, syenite and andesite to alkali basalt (Table 6; Figs. 10c and d). All samples exhibit similar REE patterns, are characterised by a significant flattening of HREE relative

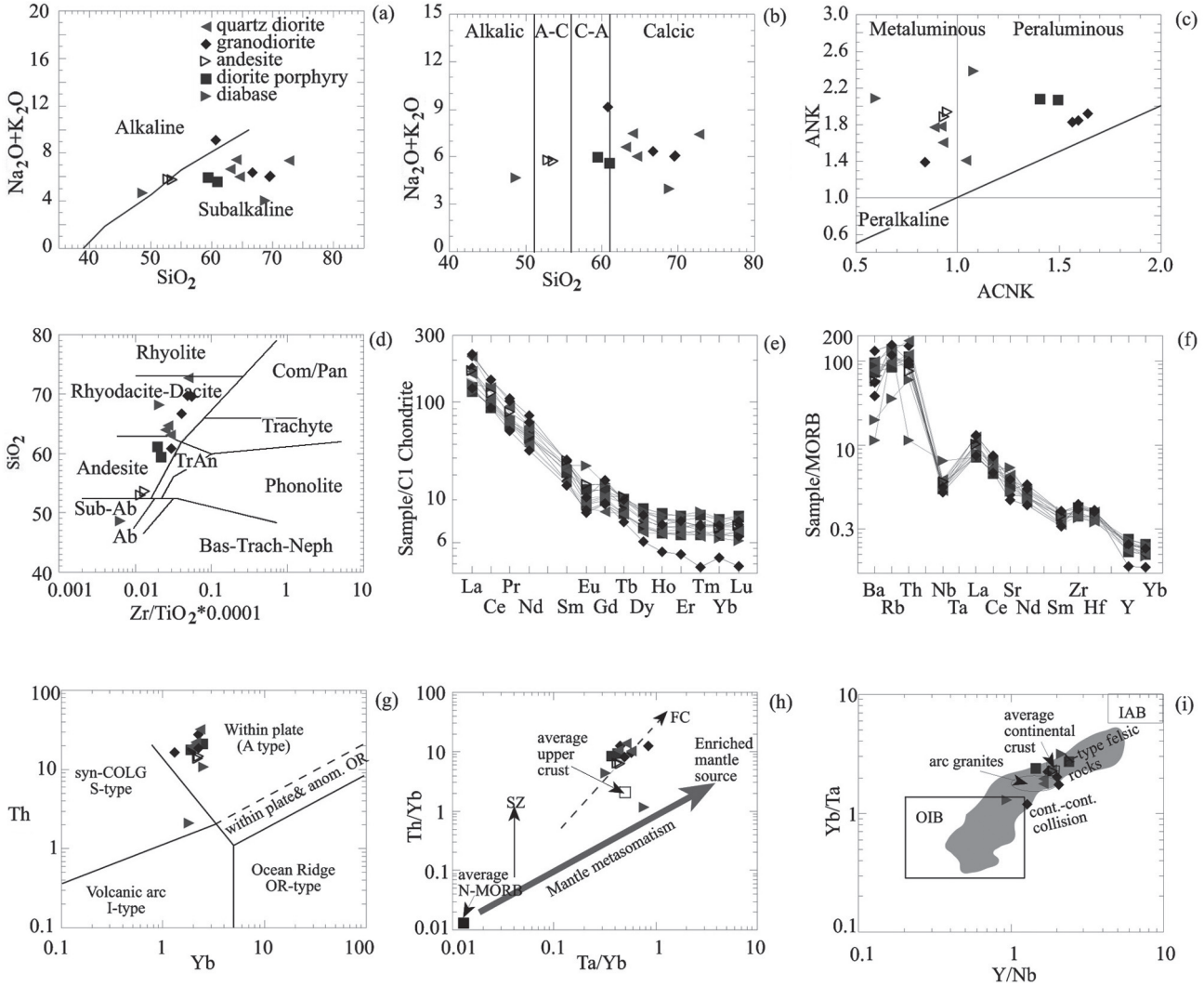

Figure 10: Geochemical classification and discrimination diagrams for igneous rocks within the Şamlı deposit: **(a)** Total alkalis versus silica (TAS) plot of Irvine and Baragar (1971); **(b)** Peacock index; **(c)** Shand index, **(d)** compositions of granitoids (Winchester and Floyd, 1977); **(e)** Rock/chondrite-normalised REE diagram for Şamlı pluton (normalising values from Nakamura, 1974); **(f)** multi-element spider diagram; **(g)** Ta-Yb diagram of Pearce, *et al.*, (1984); **(h)** Th/Yb vs Ta/Yb diagram (SZ = subduction zone trend, FC = fractional crystallisation; Pearce, 1983) showing the effect of mantle metasomatism; **(i)** Yb/Ta-Y/Nb diagram (Best and Christiansen, 2001; Whalen, *et al.*, 1987; OIB = ocean-island basalt, IAB = island-arc basalt) diagram showing the effect of crustal contamination and within-plate signature.

to the LREE, and a marked depletion in Eu, except for the dolerite (Fig. 10e). All samples show significant flattening of HREE patterns relative to LREE, while the LIL elements are enriched with respect to those that are HFS (Fig. 10f). They also show strong negative Nb and Ba, and positive Rb, Th and La anomalies (Fig. 10f).

They mostly plot in the VAG (volcanic arc granite) field (Fig. 10g; Pearce *et al.*, 1984). In general, the granitoids display a geochemical trend more akin to A-type felsic rocks that show a linear distribution between OIB and IAB (Fig. 10i). The Th/Yb vs Ta/Yb diagram (Fig. 10h) suggests the Şamlı pluton may be derived from a mantle source which was either previously enriched by small-degree partial melts (displacement along the mantle array), or from a melt that underwent significant fractional crystallisation. The displacement of all samples away from the mantle array towards a higher Th/Yb ratio (Fig. 10h) may also be indicative of enrichment by an older subduction event, as well as crustal components. The multi-element patterns of felsic and mafic end members in spidergrams and REE diagrams along with Th/Yb vs Ta/Yb and Yb/Ta vs Y/Nb suggest that assimilation-combined fractional crystallisation played an important role in magma composition (Figs. 10h and i). Similarly, higher Th/Yb, with increasing Ta/Yb and negative Nb anomalies (Figs. 10f and h), suggest an enriched mantle source, accompanied by fractional crystallisation for the granitoids. In addition, enrichment in Th within a restricted Yb range would suggest that the Şamlı pluton was formed in an extension-dominated crustal setting. This is in agreement with the previous works in the whole WAEP. The evolution of magmatism in the WAEP is closely associated with the tectonic evolution of the region, represented by a transition from a compressional to extensional regime in the Late Oligocene (Seyitoğlu *et al.*, 1992, Seyitoğlu and Scott, 1996) to Late Miocene (Dewey and Şengör, 1979; Şengör *et al.*, 1985). This evolution generated rocks with distinct petrogenetic affinities, ranging from calc-alkaline during the Oligocone to Middle Miocene, to ultrapotassic to sodic-alkaline in the Late Miocene to Quaternary. Okay and Satir (2000) suggested that the 23 to 20 Ma magmatic rocks were formed during core-complex development due to roll-back of the subducted slab along the Aegean subduction zone. However, Innocenti *et al.* (2005) favours a slab-pull for the prolonged extension within the entire western Anatolian province.

Geochronology

The Rb/Sr biotite whole rock geochronology of the Şamlı pluton yielded an age of 23.5±1.5 to 18.4±2.2 Ma (Ataman, 1974; Karacık *et al.*, 2008). This age overlaps with other intrusive rocks within the WAEP associated with iron-, iron-copper-skarns (Ayazmant and Evciler skarn deposits), and some of the leucocratic biotite-phyric granites that formed during core-complex development due to slab-roll-back or slab-pull along the Aegean subduction zone (Okay and Satır, 2000; Innocenti *et al.*, 2005). However, there is no available geochronologic data for the alteration of the Şamlı deposit.

Alteration

Alteration associated with the Şamlı mineralisation is characterised by at least three successive stages related to the formation of magnetite ore. The resultant alteration assemblages are classified as pre-, syn- and post-magnetite. In general, the alteration and main magnetite orebodies tend to be localised along northeast-southwest trend directions. The pre-magnetite stage includes: (1) a Ca-Fe assemblage, characterised by pyroxene (diopside±hedenbergite), and (2) Na-Ca alteration dominated by albite±scapolite (albitic alteration) and garnet. The syn-magnetite alteration is represented by assemblages consisting of tremolite-epidote and magnetite, with biotite, occasionally altered to chlorite. The post-magnetite assemblage overprints both the main Na-Ca phase and the magnetite mineralisation. This latter alteration phase also hosts sulphide and oxidised sulphide mineralisation and gold, with a mineralogy of quartz-calcite-pyrite-chalcopyrite-hematite-malachite-azurite-native copper.

The pre-magnetite Ca-Fe alteration, mainly characterised by pyroxene, is very sporadic, and may be obscured by late albite and garnet. The pyroxenes are mostly diopsidic to hedenbergitic in composition, and can only be recognised under the microscope. The term "albitic alteration" refers to assemblages dominantly occurring as 1 to 5 cm thick albite-veins, as well as albite patches or brecciated rock masses replaced by a calc-silicate (mostly garnet) matrix. Albitic alteration commonly extends from the diorite porphyry-diorite towards the metadolerite and metapelitic rocks, with an increase in intensity at the immediate contact zone. Away from the contact, towards the metadolerite and metapelitic rocks, the frequency of albite veining decreases, suggesting the albitic alteration zone represents deeper and/or central parts of the pluton (Barton *et al.*, 1991; Hitzman *et al.*, 1992; Hitzman, 2000; Barton and Johnson 1996). Albite, the dominant mineral of the alteration zone, is locally accompanied by scapolite, mostly converted from plagioclase. The albitic alteration and albite veins are replaced by garnet, and preserved as patches or islands within the garnet-rich rocks. Locally, hydrothermal brecciation appears to contribute to the transition from albitic to garnet alteration. Garnet is the dominant constituent of the pre-ore Na-Ca-Fe alteration. It is easily recognised in the field by the appearance of dark brown to red garnet veins/veinlets and patches in the rocks which are rich in albite, pyroxene and amphibole. The garnet-rich patches/pockets also show a close spatial relationship with irregular pockets and veins of magnetite and hematite, both of which are more concentrated along the contact between the Şamlı pluton and the metadolerite and recrystallised limestone.

The syn-magnetite alteration, which, apart from sporadic biotite concentrations, comprises an assemblage of epidote-chlorite±tremolite that occurs as veins, lenses and pockets within the pre-magnetite Na-Ca envelope. Although intense chloritisation has resulted in the almost total destruction of hydrothermal biotite, erratic occurrences of biotite are found in spatial association with magnetite pockets. Epidote is the dominant constituent of the syn-magnetite alteration and mostly occurs as predominantly northeast-striking veins that range from a few to 20 cm in thickness. The post-magnetite alteration comprises chalcopyrite, (+epidote+actinolite), hematite-limonite and copper-rich (malachite, azurite and native copper) assemblages. Magnetite bodies are replaced by sulphide minerals, including small pods which comprise minor amounts of chalcopyrite, pyrite, bornite, galena, sphalerite, bismuth, cobaltite, muschketowite and gold (Murakami, 2005). Chalcopyrite, being the most common sulphide, is usually observed as micro-veinlets, together with pyrite, overprinting or replacing magnetite. The amount of chalcopyrite, which ranges from 0.3% to >1%

and occurs as veinlets within the magnetite, increases perceptibly with increasing depth in the open pit. Copper-carbonates (malachite and azurite) are the dominant form of copper mineralisation on the upper benches of the pit, whereas native copper is significant on the lower (deeper) levels.

Structural Controls

The bulk of the alteration and the majority of the albite, garnet and magnetite veins associated with the Şamlı deposits have a northeast strike, while epidote veins, connected to the post-ore stage, strike northwest. Vein and pod-like magnetite bodies are aligned along two parallel fractures striking ENE-WSW to east-west and dipping to the south. This trend most likely follows the dominant direction of the loci of emplacement of Tertiary magmatism within the WAEP.

Conclusions

A diverse suite of epigenetic iron oxide-copper±gold-bearing deposits have been recognised in Turkey. The pervasive Na-Ca and Ca-Fe alteration hosting iron-oxide, copper and gold mineralisation at the Divriği (Sivas), Hasançelebi (Malatya) and Şamlı (Balikesir) deposits are consistent with models which suggest that these are IOCG-style deposits, structurally controlled by crustal scale faults and shear zones. The wall- and host-rocks are intensely altered and display a deposit-scale zonation

Table 6: Results of geochemical analysis of selected samples from the Şamlı pluton. nd = not detected.

Sample	181	625	626	S16	S24	S53	S54	S55	S13	S16	S19	S6
SiO_2	60.7	64.6	53.6	66.7	61.0	59.4	48.7	69.7	63.1	64.0	68.8	53.0
Al_2O_3	16.7	14.9	15.8	15.7	16.1	17.2	14.2	14.9	16.3	16.1	13.9	16.5
Fe_2O_3	3.1	4.9	9.5	4.9	6.5	6.7	10.6	3.1	5.2	4.8	6.0	9.8
MgO	2.1	2.3	4.5	0.7	2.7	2.9	8.8	1.1	2.3	2.0	0.8	4.5
CaO	4.4	4.6	4.7	0.8	2.0	1.8	9.4	0.8	4.7	4.1	3.7	4.9
Na_2O	3.8	3.3	3.8	2.3	3.1	3.4	3.1	2.8	3.5	3.4	3.0	4.0
K_2O	5.3	2.8	1.9	4.1	2.5	2.6	1.6	3.2	3.1	4.0	1.0	1.9
TiO_2	0.5	0.5	1.1	0.4	0.7	0.8	2.0	0.3	0.5	0.5	0.6	1.1
P_2O_5	0.2	0.2	0.3	0.2	0.2	0.3	0.2	0.1	0.1	0.2	0.1	0.3
MnO	0.1	0.1	0.2	0.1	0.1	0.1	0.1	0.0	0.1	0.1	0.1	0.1
TOTAL	99.9	101.6	102.1	99.7	99.2	99.6	99.6	99.8	99.7	99.7	99.7	99.7
Ba	1890	1110	834.0	1252.0	1049.0	1362.0	163.0	792	1125	1407	286.0	831.0
Sc	nd	nd	nd	7.0	12.0	10.0	30.0	6.0	11.0	9.0	15.0	20.0
Co	8.0	11.4	24.0	11.8	20.3	24.9	35.2	14.4	17.2	17.2	69.0	26.2
Cs	2.4	4.4	4.0	9.5	2.9	5.4	37.3	9.1	5.5	4.0	1.7	4.3
Ga	19.3	15.9	18.1	18.3	16.0	17.6	16.8	16.4	16.6	16.3	17.1	18.2
Hf	4.6	3.6	3.9	4.7	4.1	4.5	3.5	4.6	4.6	4.1	3.5	4.0
Nb	11.3	10.3	12.2	12.9	10.9	12.7	23.2	10.6	11.5	13.9	11.9	12.9
Rb	171.5	105.5	130.0	171.7	95.3	94.8	155.1	171.7	110.0	147.5	39.9	138.3
Sr	472.0	460.0	527.0	357.4	392.1	465.5	658.4	309.5	483.7	533.1	342.6	600.6
Ta	1.1	0.9	0.9	1.0	0.9	0.8	1.4	1.1	1.1	1.2	0.8	1.0
Th	18.4	22.2	13.9	27.6	20.8	17.6	2.1	18.3	19.6	32.3	10.9	14.6
U	4.9	4.2	6.1	6.0	4.9	4.0	0.7	5.3	6.9	9.8	1.8	6.2
V	127.0	93.0	181.0	76.0	139.0	129.0	298.0	48.0	103.0	92.0	79.0	210.0
Zr	156.0	132.0	141.0	171.2	128.6	162.4	125.9	165.6	154.7	128.4	121.8	129.9
Y	22.6	19.2	22.7	22.4	26.2	18.5	21.7	21.8	18.8	22.7	25.4	24.5
Mo	nd	nd	nd	1.7	0.6	0.3	nd	0.1	0.2	0.3	nd	0.1
Cu	225.0	9.0	6.0	493.7	3892.7	102.7	7.1	47.4	10.4	2.4	373.6	8.2
Pb	31.0	65.0	54.0	108.9	52.3	132.8	4.8	20.6	8.1	4.6	16.9	25.6
Zn	75.0	79.0	228.0	236.0	99.0	85.0	24.0	59.0	24.0	30.0	38.0	177.0
Ni	49.0		24.0	11.3	121.4	17.2	69.9	8.5	3.8	2.5	87.2	20.7
As	nd	nd	nd	47.8	7.4	7.6	10.8	4.5	1.4	0.5	2.2	4.2
Sb	nd	nd	nd	1.0	0.6	1.2	1.4	0.9	nd	nd	0.1	0.3
La	52.2	38.0	32.4	50.8	30.1	28.0	28.3	41.6	39.4	49.9	31.9	39.8
Ce	88.4	65.4	61.2	88.7	55.5	58.2	58.7	63.1	62.3	78.1	77.6	71.7
Pr	9.7	6.7	6.8	10.1	6.6	6.8	7.0	7.2	7.1	9.0	7.5	8.1
Nd	33.4	22.6	26.2	37.4	25.6	26.8	29.3	26.9	23.4	31.6	27.0	31.7
Sm	6.0	4.1	5.4	5.8	4.9	4.8	5.4	4.2	4.1	5.0	5.3	5.8
Eu	1.2	1.1	1.5	1.3	1.4	1.1	2.0	1.0	1.0	1.2	1.1	1.5
Gd	5.7	4.3	5.4	4.9	4.8	4.1	5.4	3.8	3.4	4.4	4.3	5.3
Tb	0.8	0.6	0.8	0.7	0.8	0.6	0.8	0.6	0.6	0.7	0.8	0.8
Dy	4.0	3.4	4.1	3.7	4.4	3.2	4.3	3.3	3.0	3.7	4.2	4.1
Ho	1	1	1	1	1	1	1	1	1	1	1	1
Er	2	2	2	2	3	2	2	2	2	2	3	2
Tm	nd	nd	nd	nd	nd	nd	nd	nd	nd	nd	nd	nd
Yb	2	2	2	2	2	2	2	2	2	2	3	2
Lu	nd	nd	nd	nd	nd	nd	nd	nd	nd	nd	nd	nd

at both Divriği and Şamlı, and a region-scale zonation at Hasançelebi. Structural control is most prominent at Hasançelebi and Divriği. These deposits all exhibit distinct sodic-calcic alteration, overprinted by a later potassic phase. The peripheral, distal alteration zone is characterised by scapolite-diopside-garnet-actinolite at Hasançelebi; scapolite-garnet-diopside at Divriği; and albite-garnet-pyroxene at Şamlı. The proximal alteration zone is represented by phlogopite-K feldspar at Divriği and Hasançelebi; and by epidote-tremolite and biotite in the Şamlı district. The iron oxide mineralisation occurs as massive magnetite, accompanied by K feldspar and biotite-epidote and/or a phlogopite-rich zone, superimposed on scapolite-garnet or albite-garnet alteration. Martitised magnetite, limonite, silica and sulphide mineralisation occur as replacements of the main magnetite bodies. These deposits all contain distinct elemental associations of Fe-Cu-Au ± Ag, Bi, Ba, Co, Th, U, LREE. Concentrations have been recorded as high as 5.7 to 8.8 ppm Au, and up to 5% Cu (ore grade samples) at Şamlı; <1 ppm Au, and up to 1.5 to 2% Cu at Divriği; and a maximum of 0.7 ppm Au, and about 1% at Hasançelebi.

Latest Cretaceous (75 to 71 Ma) magmatism throughout easternmost central Anatolia, and the immediately adjoining regions, is generally considered to have taken place under variably extensional conditions in response to retreating subduction boundaries (slab roll-back) along the Bitlis-Zagros subduction zone (Kuscu *et al.*, 2008). However, Oligocene to Miocene magmatism (23.5 to 22.3 to 18.4 Ma; Ataman, 1974; Watanabe *et al.*, 2003; Isik *et al.*, 2004; Ring and Collins, 2005; Innocenti *et al.*, 2005, Karacık *et al*., 2008) in western Anatolia, is generally accepted to have been formed during core-complex (Okay and Satir, 2000) to slab-pull (Innocenti *et al.*, 2005) along the Aegean subduction complex. Based on these ages and a regional compilation, favourable time periods for IOCG-style mineralisation are 74 to 69 Ma and 23 to 18 Ma in central and western Anatolia respectively. These periods represent crustal-scale extension due to post-collisional roll-back of the subducting slab beneath the Malatya-Keban platform within the Bitlis-Zagros subduction zone (central-eastern Anatolia) and Aegean subduction complex (western Anatolia). The most prospective settings for IOCG-style deposits in Turkey are post-collisional, late-orogenic extensional settings, where Latest Cretaceous to Paleocene (central Anatolia), to Oligocene (western Anatolia), alkaline to calc-alkaline magmas are emplaced into shallow crustal levels, intruding lacustrine to deep marine sedimentary sequences. Extensive, brittle fault systems, including the northeast-southwest oriented Malatya-Ovacik (MOFZ), Yakapinar-Goksu-Sariz (GSFZ), Kangal-Cetinkaya and Central Anatolian (CAFZ) fault zones in central Anatolia, and/or ductile/brittle shear zones and deeply penetrating detachment faults trending east-west to northeast-southwest in western Anatolia, appear to control the spatial association of sodic alteration zones and the emplacement/exposure of causative magmatic rocks.

Acknowledgements

This work is part of M.Sc and Ph.D. studies by Erkan Yilmazer, and received financial support from the Scientific and Technological Research Council of Turkey (TUBITAK; grant no. CAYDAG 103Y023), Middle East Technical University (METU)-BAP-03-09-2007-04 project and Turkish Petroleum Corp. (TPAO). We would like to express our sincere thanks to these organisations.

References

Akyurek, B. and Soysal, Y., 1983 - Biga yarimadasi guneyinin (Savastepe- Kirkagac-Bergama-Ayvalik) temel jeoloji özellikleri [Basic geological features of the region south of the Biga Peninsula (Savastepe-Kirkagac-Bergama-Ayvalik)]; *Maden Tetkik ve Arama Enstitusu,* Bulletin 95/96, pp. 1-13 (*in Turkish with English abstract*).

Angus, D.A., Wilson, D.C., Sandvol, E. and Ni, J.F., 2006 - Lithospheric structure of the Arabian and Eurasian collision zone in eastern Turkey from S-wave receiver functions; *Geophysical Journal International,* v. 166, pp. 1335-1346.

Ataman, G., 1974 - Revue geochronoloqique, des massifs plutoniques et metamorphiques de I'Anatolie; *Hacettepe Bulletin of Natural Sciences and Engineering,* v. 3, pp. 518-523.

Ay, Y., Yıldırım, S., Dumanlılar, O., Turgut, O., Tablacı, A., Yıldız, H. and Dumanlılar., H., 2004 - An example of Olympic Dam-type Fe oxide-Cu-Au-(Ag-Ba-U-Th-REE) deposits from Turkey: Hasançelebi Fe deposit [abs.]; *57th Geological Congress of Turkey, Ankara*, Abstracts with Programs*,* pp. 107-108.

Barton, M.D., Hassanzadeh, J., Battles, D.A. and Marikos, M.A., 1991 - Magnetite-apatite-REE mineralization in the Great Basin [abs]; *Geological Society of America,* Abstracts with Programs, v. 23, p 292.

Barton, M.D. and Johnson, D.A, 1996 - Evaporitic source model for igneous related Fe oxide-(REE-Cu-Au-U) mineralization; *Geology,* v. 24, pp. 259-262.

Bowers, T.S. and Taylor, H.P., Jr. 1985 - An integrated chemical and stable isotope model of the origin of midocean ridge hot spring systems; *Journal of Geophysical Research,* v. 90, pp. 12583-12606.

Bozkurt, E., 2001 - Neotectonics of Turkey – a synthesis; *Geodinamica Acta,* v. 14, pp. 3-30.

Bozkurt, E. and Park, R.G., 1997 - Evolution of a mid-Tertiary extensional shear zone in the southern Menderes massif, western Turkey; *Bulletin of Geological Society of France*, v. 168, pp. 3-14.

Bozkurt, E. and Mittwede, S.K., 2001 - Introduction to the Geology of Turkey-a synthesis; *International Geology Review*s, v. 43, pp. 578-591.

Bozkurt, E. and Oberhansli, R., 2001 - Menderes Massif (Western Turkey): structural, metamorphic and magmatic evolution-a synthesis; *International Journal of Earth Sciences*, v. 89, pp. 679-708.

Boztuğ, D. and Harlavan, Y., 2007 - K-Ar ages of granitoids unravel the stages of Neo-Tethyan convergence in the eastern Pontides and central Anatolia, Turkey; *International Journal of Earth Sciences,* v. 97, pp. 585-599 (doi: 10.1007/s00531-007-0176-0).

Boztuğ, D., Harlavan, Y., Arehart, G.B., Satır, M. and Avcı, N., 2007 - K-Ar age, whole rock and isotope geochemistry of A-type granitoids in the Divriği-Sivas region, eastern-central Anatolia, Turkey; *Lithos,* v. 97, pp. 193-218.

Clayton, R.N., O'Neil, J. R. and Mayeda, T.K., 1972 - Oxygen isotope exchange between quartz and water; *Journal of Geophysical Research,* v. 77, pp. 3057-3067.

Çolakoğlu, A.R. and Murakami, H., 2006 - Karakaya Kompleks Zonu İçinde Gözlenen Şamlı ve Ayazmant (Balıkesir) Fe Skarn Yataklarının Jeolojisi, Parajenezi ve Oluşumu, Batı Anadolu [abs]; *59th Turkish Geological Congress, Ankara,* Abstracts with Programs*,* pp. 147-148.

DePaolo, D.J. and Daley, E.E., 2000 - Neodymium isotopes in basalts of the southwest basin and range and lithospheric thinning during continental extension; *Chemical Geology,* v. 169, pp. 157-185.

Dewey, J.F. and Şengör, A.M.C., 1979 - Aegean and surrounding regions: complex multiplate and continuum tectonics in a convergent zone; *Geological Society of America Bulletin,* v. 90, pp. 84-92.

Doglioni, C., Agostini, S., Crespi, M., Innocenti, F., Maetti, P., Riguzzi, F. and Savascin, M.Y., 2002 - On the extension in western Anatolia and the Aegean sea. In: Rosenbaum, G. and Lister, G. S. Reconstruction of the evolution of the Alpine-Himalayan Orogen; *Journal of the Virtual Explorer,* v. 8, pp. 161-176.

Faccenna, G., Bellier, O., Martinod, J., Piromallo, C. and Regard, V., 2006 - Slab detachment beneath eastern Anatolia: A possible cause for the formation of the North Anatolian fault; *Earth and Planetary Science Letters,* v. 242, pp. 85-97.

Göncüoğlu, M.C., Dirik, K. and Kozlu, H., 1997 - Pre-Alpine and Alpine Terranes in Turkey: explanatory notes to the terrane map of Turkey; *Annales Geologique de Pays Hellenique*, v. 37, pp. 515-536.

Göncüoğlu, M.C., Turhan, N., Şentürk, K., Özcan, A., Uysal, S. and Yalınız, M.K., 2000 - A geotraverse across northwestern Turkey: tectonic units of the Central Sakarya region and their tectonic evolution; *in*: Bozkurt, E., Winchester, J.A. and Piper, J.D., (eds.), Tectonics and Magmatism in Turkey and the Surrounding Area; *Geological Society, London, Special Publications,* v. 173, pp. 139-162.

Günalay, M.E., 1968 - Report of Operating iron ore in the Şamlı (Balıkesir); *General Directorate of Mineral Research and Exploration,* Rep. No: 4332 Ankara (*in Turkish*).

Gürer Ö.F., 1996 - Geological position and the genesis of Hasançelebi alkaline magmatism at the eastern Taurides (NW Malatya); *Turkish Journal of Earth Sciences,* v. 5, pp. 71-88.

Gürer, Ö.F., 1992 - Hekimhan-Hasançelebi (Malatya) Dolayının Jeoloji İncelemesi; Thesis *İ.Ü. Fen Bilimleri Enstitüsü Dissertation*, 323p. (*In Turkish with English abstract*)

Hafkenscheid, E., Wortel, M.J.R. and Spakman, W., 2006 - Subduction history of the Tethyan region derived from seismic tomography and tectonic reconstructions; *Journal of Geophysical Research,* v. 111, B08401, (doi:10.1029/2005JB003791).

Hitzman, M.W., Oreskes, N. and Einaudi, M.T., 1992 - Geological characteristics and tectonic setting of Proterozoic iron oxide (Cu-U-Au-REE) deposits; *Precambrian Research,* v. 58, pp. 241-287.

Hitzman, M.W., 2000 - Iron oxide-Cu-Au deposits: what, where, when, and why; *in*: Porter T.M., (ed.), Hydrothermal Iron Oxide Copper-gold and Related Deposits: a Global Perspective, *PGC Publishing, Adelaide*, v. 1, pp. 9-25.

Innocenti, F., Agostini, T,S., Di Vincenzo, G., Doglioni, C., Manetti, P., Savascin, M.Y. and Tonarini, S., 2005 - Neogene and Quaternary volcanism in Western Anatolia:Magma sources and geodynamic evolution; *Marine Geology,* v. 221, pp 397-421 (doi:10.1016/j.margeo.2005.03.016).

Irvine T.N. and Baragar, W.R.A., 1971 - A guide to the chemical classification of the common volcanic rocks; *Canadian Journal of Earth Sciences,* v. 8, pp. 523-548.

Isik, V., Tekeli, O. and Seyitoglu, G., 2004 - The $^{40}Ar/^{39}Ar$ age of extensional ductile deformation and granitoid intrusions in the northern Menderes core complex: implications for the initiation of extensional tectonics in western Turkey; *Journal of Asian Earth Sciences*, v. 23, pp. 555-566.

Jahn, B.M., Wu, F., Lo, C.H. and Tsai, C.H., 1999 - Crust-mantle interaction induced by deep subduction of the continental crust: geochemical and Sr-Nd isotope evidence from post-collisional mafic-ultramafic intrusions of the northern Dabie complex, central China; *Chemical Geology,* v. 157, pp. 119-146.

Jolivet, L., Famin, V., Mehl, C., Parrat, T., Aubourg C., Hebert R. and Philippot P., 2004 - Progressive strain localisation, crustal-scale boudinage and extensional metamorphic domes in the Aegean Sea; *Geological Society of America,* Special Paper, v. 380, pp. 185-210.

Karacık, Z., Yılmaz, Y., Pearce, J. A. and Ece, Ö.I., 2008 - Petrochemistry of the south Marmara granitoids, northwest Anatolia, Turkey; *International Journal of Earth Sciences (Geol Rundsch)*, v. 97, pp. 1181-1200.

Kaymakci, N. and Kuşcu, İ., 2007 - Late Cretaceous to Recent kinematic evolution of Turkey [abs]; *European Geosciences Union 2007 Geophysical Research Abstracts*, v. 9, p. 5426, (SRef-ID 1607-7962/gra/EGU2007-A-05426)

Keskin, M., 2003 - Magma generation by slab steepening and break off beneath a subduction-accretion complex: An alternative model for collision-related volcanism in eastern Anatolia, Turkey; *Geophysical Research Letters,* v. 30, no. 24, 8046, (doi:10.1029/ 2003GL018019).

Ketin, İ., 1966 - Anadolu'nun tektonik birlikleri; *Maden Tetkik ve Arama Bulletin,* v. 66, pp. 20-34. (*in Turkish*)

Koçyiğit, A., 1987 - Tectono-stratigraphy of the Hasanoglan (Ankara) region: evolution of the Karakaya orogen; *Yerbilimleri,* v. 14, pp. 269-293.

Kohn, M.J. and Parkinson, C.D., 2002 - Petrologic case for Eocene slab break off during the Indo-Asian collision; *Geology,* v. 30, pp. 591-594.

Kosal, C., 1973 - Divriği A-B-C demir yataklarının jeolojisi ve oluşumu üzerine çalışmalar; *Maden Tetkik ve Arama Bulletin,* v. 81, pp. 1-22. *(in Turkish)*

Kuru, G., Kuşcu, İ., Şalış B., Yılmazer, E. and Demirela, G., 2006 - Hasançelebi (Malatya) demir oksit yataklarının oluşum koşulları: mikrotermometrik bir yaklaşım; *Maden Tetkik Arama Bulletin,* v. 132, pp. 101-111 (*In Turkish with English abstract*).

Kusakabe, M. and Robinson, B.W., 1977 - Oxygen and sulfur isotope equilibria in the $BaSO_4$-HSO_4^--H_2O system from 110 to 350°C and applications; *Geochimica et Cosmochimica Acta,* v. 41, pp. 1033-1040.

Kuşcu, İ., Gencalioglu-Kuşcu, G., Tosdal, R.M., Ullrich, T. and Friedman, R., 2007d - Link between magmatism and subduction-related events in eastern-southeastern Turkey [abs]. *Geophysical Research Abstracts,* v. 9, 4814, (SRef-ID: 1607-7962/gra/EGU2007-A-04814).

Kuşcu, İ., 2003 - Fe-oksit-Cu-Au-REE (Olympic Dam) Tipi Yataklar: Genel Özellikleri-Oluşum Modeli ve Orta Anadolu Potansiyelinin Bir Değerlendirmesi. [abs]; 20th Geological symposium of Süleyman Demirel Üniversitesi Jeoloji Mühendisliği Bölümü, *TMMOB Jeoloji Mühendisleri Odası Yayınları,* Abstracts with Programs, v. 73, p 176.

Kuşcu, İ., Gençalioğlu-Kuşcu, G. and Tosdal, R.M., 2007a - Tectonomagmatic-metallogenic framework of mineralization events in the southern NeoTethyan arc, southeastern Turkey; *Proceedings of 9th Biennial SGA Meeting, Mineral Exploration and Research*: *Digging Deeper*, Dublin, pp. 1347-1350.

Kuşcu, İ., Gençalioğlu-Kuşcu, G., Tosdal, R.M., Ullrich, T. and Friedman, R., 2008 - Magmatism in the southeastern Anatolian orogenic belt: transition from arc to post-collisional setting in an evolving orogen. *in* Sosson, M. and Kaymakci, N., (eds.), Basins and Tectonic Evolution of the Caucasus and the Eastern Anatolia regions; *Geological Society of London, Special publication,* [in press].

Kuşcu, İ., Yılmazer, E, Demirela, G., Güleç, N., Kuşcu, G., Kaymakcı, N., Gökçe, H., Şalış, B. and Marschik, R., 2007c - Hasançelebi-Hekimhan (Malatya) Bölgeleri Demiroksit Yataklarının Demir Oksit-Bakır-Altın (DOBA) Yatakları Açısından İncelenmesi ve Bakır-Altın Potansiyellerinin Araştırılması *TUBITAK Project-CAYDAG 103Y023*, 190p. (*in Turkish with English abstract*)

Kuşcu, İ., Yılmazer, E. and Demirela, G., 2002 - Sivas-Divriği Bölgesi Skarn Tipi Demir Oksit Yataklarına Fe-oksit-Cu-Au (Olympic Dam tipi) Perspektifinden Yeni Bir Bakış (Sivas-Divriği skarn-type Fe-oxide deposits in view of Fe-oxide-Cu-Au (Olympic Dam type deposits); *Türkiye Jeoloji Bulteni,* v. 45, no. 2, pp. 33-46. (*in Turkish with English abstract*)

Kuşcu, İ., Yılmazer, E. and Demirela, G., 2002 - Sivas-Divriği Bölgesi Skarn Tipi Demir Oksit Yataklarına Fe-oksit-Cu-Au (Olympic Dam tipi) Perspektifinden Yeni Bir Bakış; *Turkiye Jeoloji Kurumu Bulletin*, v. 45, no. 2, pp. 33-47. *(in Turkish)*

Kuşcu, İ., Yılmazer, E. and Demirela, G., 2007b - Iron oxide-copper±gold deposits in Turkish Tethyan collage. *Proceedings of 9th Biennial SGA Meeting, Mineral Exploration and Research:Digging Deper*, Dublin, pp. 853-857.

Kuşcu, İ., Yilmazer, E., Demirela, G. and Gökçe, H., 2005a - Fe-Oxide-Cu-Au potential of some "skarn-type" Fe-oxide deposits in central and western Anatolia; *Proceedings of the Geology, Mining and current problems of Turkish Iron Deposits*, pp. 181-206. (*in Turkish with English abstract*)

Kuşcu, I., Yılmazer, E., Demirela, G. and Gökçe, H., 2005b - Orta ve Batı Andalu'daki Bazı Skarn-Tipi Fe-Oksit-Cu-Au (DOBA) Potansiyeli; *Proceedings of Türkiye Demir Yataklari Jeolojisi, Madenciliği ve Mevcut Sorunları Sempozyumu*, pp. 179-204. *(in Turkish)*

Le Maitre, R.W., Bateman, P., Dudek, A., Keller, J., Lameyre, J., Le Bas, M.J., Sabine, P.A., Schmid, R., Sorensen, H., Streckeisen, A., Woolley, A.R. and Zanettin, B., 1989 - A Classification of Igneous Rocks and Glossary of Terms; *Blackwell, Oxford*, 193p.

Leo, G.W. and Genc, M.A., 1986 - Geology and iron deposits of the Şamlı area, Balıkesir Province, Turkey, *MTA,* Report 4928.

Marschik, R., Spikings, R. and Kuşcu, İ., 2008 - Geochronology and stable isotope signature of alteration related to hydrothermal magnetite ores in Central Anatolia, Turkey; *Mineralium Deposita*, v. 43, pp. 111-124 (doi 10.1007/s00126-007-0160-4).

MTA, 1964 - Iron ore deposits in Turkey, *MTA,* Publication no. 118, 56p.

Murakami, H., 2005 - How to study skarn type Deposits; A short term expert seminar, submitted to MTA (Turkey), *Shortcourse material*, 12p.

Okay, A. and Satir, M. 2000 - Coeval plutonism and metamorphism in a latest Oligocene metamorphic core complex in northwest Turkey; *Geological Magazine,* v. 137, no. 5, pp. 495-516.

Okay, A. and Tuysuz, O., 1999 - Tethyan sutures of northern Turkey; *in:* Durand, B., Jolivet, L., Horvath, F. and Serrane, M., (eds.), The Mediterranean Basins: Tertiary Extension within the Alpine Orogen. *Geological Society, London, Special Publications*, v. 156, pp. 475-515.

Okay, A.İ. and Göncuoğlu, M.C., 2004 - The Karakaya Complex: A review of data and concepts; *Turkish Journal of Earth Sciences,* v. 13, pp. 77-95.

Okay, A.I., Kaslılar-Ozcan, A., Imren, C., Boztepe-Guney, A., Demirbag, E. and Kuşcu, I., 2000 - Active faults and evolving strike-slip basins in the Marmara sea, Northwest Turkey: a multichannel seismic reflection study; *Tectonophysics,* v. 321, pp. 189-218.

Okay, A.İ., Siyako, M. and Bürkan, K.A., 1990 - Geology of the Biga Peninsula and its tectonic evolution; *Turkish Association of Petroleum Geologists Bulletin*, v. 2, pp. 83-121. (*in Turkish*)

Öztürk, H. and Öztunali, Ö., 1993 - Divriği demir yatakları üzerine genç tektonizma etkileri ve sonuçlan; *Türkiye Jeoloji Bulletin,* v. 8, pp. 97-106. (*in Turkish with English abstract*)

Parlak, O., Yilmaz, H. and Boztug, D., 2006 - Origin and tectonic significance of the metamorphic sole and isolated dykes of the Divrigi ophiolite (Sivas, Turkey): evidence for slab break-off prior to ophiolite emplacement; *Turkish Journal of Earth Sciences,* v. 15, pp. 25-45.

Pearce J.A. 1983 - Role of subcontinental lithosphere in magma genesis at active continental margins; *in:* Hawkesworth, C.J. and Norry, M.J., (eds.), Continental Basalts and Mantle Xenoliths, *Shiva Publishing, Cheshire, U.K.* pp. 230-249.

Pearce, J.A., Harris, N.B.W. and Tindle, A.G., 1984 - Trace element discrimination diagrams for the tectonic interpretation of granitic rocks; *Journal of Petrology*, v. 25, pp. 956-983.

Ring, U. and Collins, A.S., 2005 - U-Pb SIMS dating of syn-kinematic granites: timing of core-complex formation in the northern Anatolide belt of western Turkey; *Journal of Geological Society of London,* v. 162, pp. 289-298.

Schimidberger, S.S. and Hegner, E., 1999 - Geochemistry and isotope systematics of calc-alkaline volcanic rocks from the Saar-Nahe basin (SW-Germany)-implications for Late Variscan orogenic development; *Contributions to Mineralogy and Petrology,* v. 135, pp. 373-385.

Sengor, A.M.C., Ozeren, S., Genc, T. and Zor, E., 2003 - East Anatolian high plateau as a mantle-supported, north-south shortened domal structure; *Geophysical Research Letter,* v. 30, no. 24, pp. TUR8.1-TUR8.4, 8045, (doi:10.1029/2003GL017858, 2003).

Sengor, A.M.C., 1987 - Tectonics of the Tethysides: Orogenic collage development in a collisional setting; *Annual Review of Earth Planet Science,* v. 15, pp. 213-244 (doi 10.1146/annurev.ea.15.050187.001241).

Şengör, A.M.C., Görür, N. and Şaroglu, F., 1985 - Strike-slip faulting and related basin formation in zones of tectonic escape: Turkey as a case study; *in:* Biddle, K.T. and Christie-Blick, N., (eds.), Strike-slip Deformation Basin Formation and Sedimentation, *Society of Economic Paleontologists and Mineralogists,* Special Publication, v. 37, pp. 227-264.

Şengör, A.M.C. and Yılmaz, Y., 1981 - Tethyan evolution of Turkey: a plate tectonic approach; *Tectonophysics,* v. 75, pp. 181-241.

Şengör, A.M.C., Yilmaz, Y. and Sungurlu, O., 1984 - Tectonics of the Mediterranean Cimmerides: nature and evolution of the western termination of Palaeo-Tethys. *in:* Dixon, J.E. and Robertson, A.H.F., (eds.), Geological Evolution of the Eastern Mediterranean, *Geological Society of London,* Special Publication, v. 17, pp. 77-112.

Şengör, A.M.C., Özeren, S., Genç, T. and Zor, E., 2003 - East Anatolia high plateau as a mantle supported, north-south shortened domal structure; *Geophysical Research Letter*, v. 30, no. 24, pp. 1-12; 8045, (doi 10.1029/2003gl017858).

Seyitoğlu, G. and Scott, B.C., 1996 - The cause of N-S extensional tectonics in western Turkey: Tectonic escape vs Back-arc spreading vs Orogenic Collapse; *Journal of Geodynamics,* v. 22, pp. 145-153.

Seyitoğlu, G., Scott, B.C. and Rundle, C.C., 1992 - Timing of Cenozoic extensional tectonics in west Turkey. *Journal of Geological Society of London*, v. 149, pp. 533-538.

Sezerer-Kuru, G., Kuşcu, İ., Şalış B., Yılmazer, E. and Demirela, G., 2006 - Hasançelebi (Malatya) demir oksit yataklarının oluşum koşulları: mikrotermometrik bir yaklaşım; *Maden Tetkik Arama Bulletin,* v. 132, pp. 101-111. (*in Turkish with English abstract*)

Sillitoe, R., 2003 - Iron oxide-copper-gold deposits: an Andean view; *Mineralium Deposita,* v. 38, pp. 787-812.

Stampfli, G.M., 2000 - Tethyan oceans; *in* Bozkurt, E., Winchester, J.A. and Piper, J.D.A., (eds.), Tectonics and Magmatism in Turkey and the Surrounding Area, *Geological Society London,* Special Publication 173, pp. 163-185.

Stampfli, G.M., 1996 - The intra-Alpine terrain; a Paleotethyan remnant in the Alpine Variscides; *in* Schmid, S.M., Frey, M., Froitzheim, N., Heilbronner, R. and Stuenitz, H., (eds.), 1996. Alpine geology; Proceedings of the Second Workshop on Alpine Geology. *Eclogae Geologicae Helvetiae,* v. 89, pp. 13-42.

Stendal, H. and Ünlü, T., (1991) Rock geochemistry of an iron ore field in the Divriği region, central Anatolia, Turkey: a new exploration model for iron ores in Turkey; *Journal of Geochemical Exploration*, v. 40, pp. 281-289.

Sun, S.S., 1982 - Chemical composition and origin of the earth's primitive mantle; *Geochimica et cosmochimica Acta,* v. 46, pp. 179-192.

Suzuoki, T. and Epstein, S., 1976 - Hydrogen isotope fractionation between OH-bearing minerals and water; *Geochimica et cosmochimica Acta,* v. 40, pp. 1129-1240.

Taylor, B.E., 1986 - Magmatic volatiles: Isotopic variation of C, H and S; *Reviews in Mineralogy,* v. 16, pp. 185-226.

Taylor, St.R. and McLennan, S.M., 1985 - The Continental Crust: its Composition and Evolution; *Blackwell Scientific Publications, Oxford,* 312p.

Tekeli, O., 1981 - Subduction complex of pre-Jurassic age, Northern Anatolia, Turkey; *Geology,* v. 9, pp. 68-72.

Ünlü, T. and Stendall, H., 1989 - Divriği Bölgesi Demir Cevheri Yataklarının Nadir Toprak Element (REE) Jeokimyası; Orta Anadolu, Türkiye; *Türkiye Jeoloji Bülteni*, v. 32, pp. 21-37. (*in Turkish with English abstract*)

Ünlü, T., Stendal, H., Makovicky, E. and Sayili, S., 1995 - Genesis of the Divriği iron ore deposit, Sivas, central Anatolia, Turkey: an ore microscopy study; *Bulletin of the Mineral Research and Exploration Institute of Turkey*, v. 117, pp. 17-28.

Van de Zedde, D.M.A. and Wortel, M.J.R., 2001 - Shallow slab detachment as a transient source of heat at mid-lithospheric depths; *Tectonics,* v. 20, pp. 868-882.

Watanabe, Y., Murakami, H. Cengiz, I, Sari, R., Kucukefe, S. and Yildirim, S., 2003 - Study on Hydrothermal Deposits and Metallogeny in Western Turkey; Japan-Turkey Project, *M.T.A.*, Progress Report No. 1 (interim report), 60p.

Whalen, J.B., Currie, K.L. and Chappell, B.W., 1987 - A-type granites: geochemical characteristics, discrimination and petrogenesis; *Contribution to Mineralogy and Petrology,* v. 95, pp. 407-419.

Winchester, J.A. and Floyd, P.A., 1977 - Geochemical discrimination of different magma series and their differentiation products using immobile elements; *Chemical Geology,* v. 20, pp. 325-343.

Wortel, M.J.R. and Spakman, W., 2000 - Subduction and slab detachment in the Mediterranean-Carpathian region; *Science,* v. 290, pp. 1910-1917.

Yılmaz, Y., Genç, Ş.C., Karacık, Z. and Altunkaynak, Ş., 2001 - Two contrasting magmatic associations of NW Anatolia and their tectonic significance; *Journal of Geodynamics,* v. 31, pp. 243-271.

Yılmazer, E., Kuşcu, I. and ve Demirela, G., 2003 - Divrigi A-B Kafa mineralizations: alteration zoning and zoning processes; *Türkiye Jeoloji Bülteni,* v. 46, no. 1, pp. 17-34. (*in Turkish with English abstract*)

Yuce, A.E., Güney, A., Elevli, B., Kökkılıç, O., Acarkan. N., Önal, G. and Demirci, A., 2005 - Hasançelebi yatağı revise fizibilitesi; *Proceedings of the Geology, Mining and Current Problems of Turkish Iron Deposits*, pp. 306-319. (*in Turkish with English abstract*)

Yurt, M.Z. and Yurt, F., 1981 - Balıkesir-Şamlı-Toybelen çevresi demir cevherleşmeleri prospeksiyon raporu. *M.T.A.,* Report 80-9/b (*in Turkish*).

Zheng, Y.F., 1993a - Calculation of oxygen isotope fractionation in hydroxyl-bearing silicates; *Earth and Planetary Science Letters,* v. 120, pp. 247-263.

Zheng, Y.F., 1993b - Calculation of oxygen isotope fractionation in anhydrous silicate minerals; *Geochimica et Cosmochimica Acta,* v. 57, pp. 1079-1091.

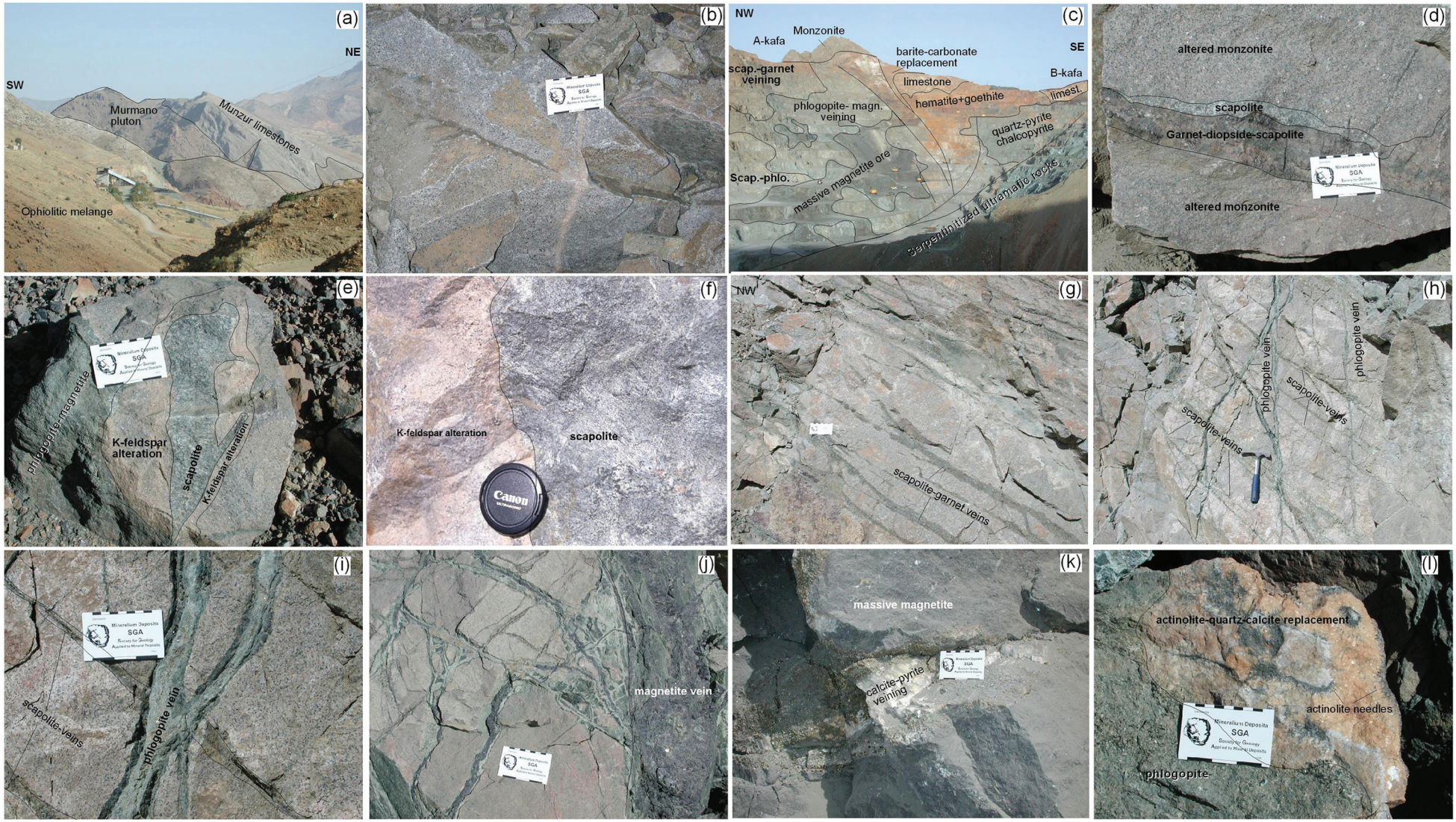

Figure 11: Characteristic features of hydrothermal alteration and magnetite ore from the Divriği IOCG deposit, and field relationship between rock units at Divriği area: **(a)** Field relationships between the ophiolitic mélange, Munzur limestone, and Murmano pluton; **(b)** Field exposure from the Murmano pluton; **(c)** General view of A- and B-kafa ore bodies looking towards ENE (see excavators for scaling); **(d)** scapolite-garnet-diopside veining; **(e)** field relationships between scapolite replaced by K-feldspar and phlogopite-magnetite alterations; **(f)** K-feldspar alteration replacing scapolite; **(g)** parallel veins of scapolite-garnet within monzonite; **(h)** phlogopite veins cutting scapolite veins; **(i)** phlogopite vein cutting the scapolite veins (close-up); **(j)** hydrothermal breccia infilled by phlogopite and magnetite; **(k)** massive magnetite replaced by late calcite-pyrite; and **(l)** late calcite-quartz-actinolite alteration replacing phlogopite-magnetite alteration.

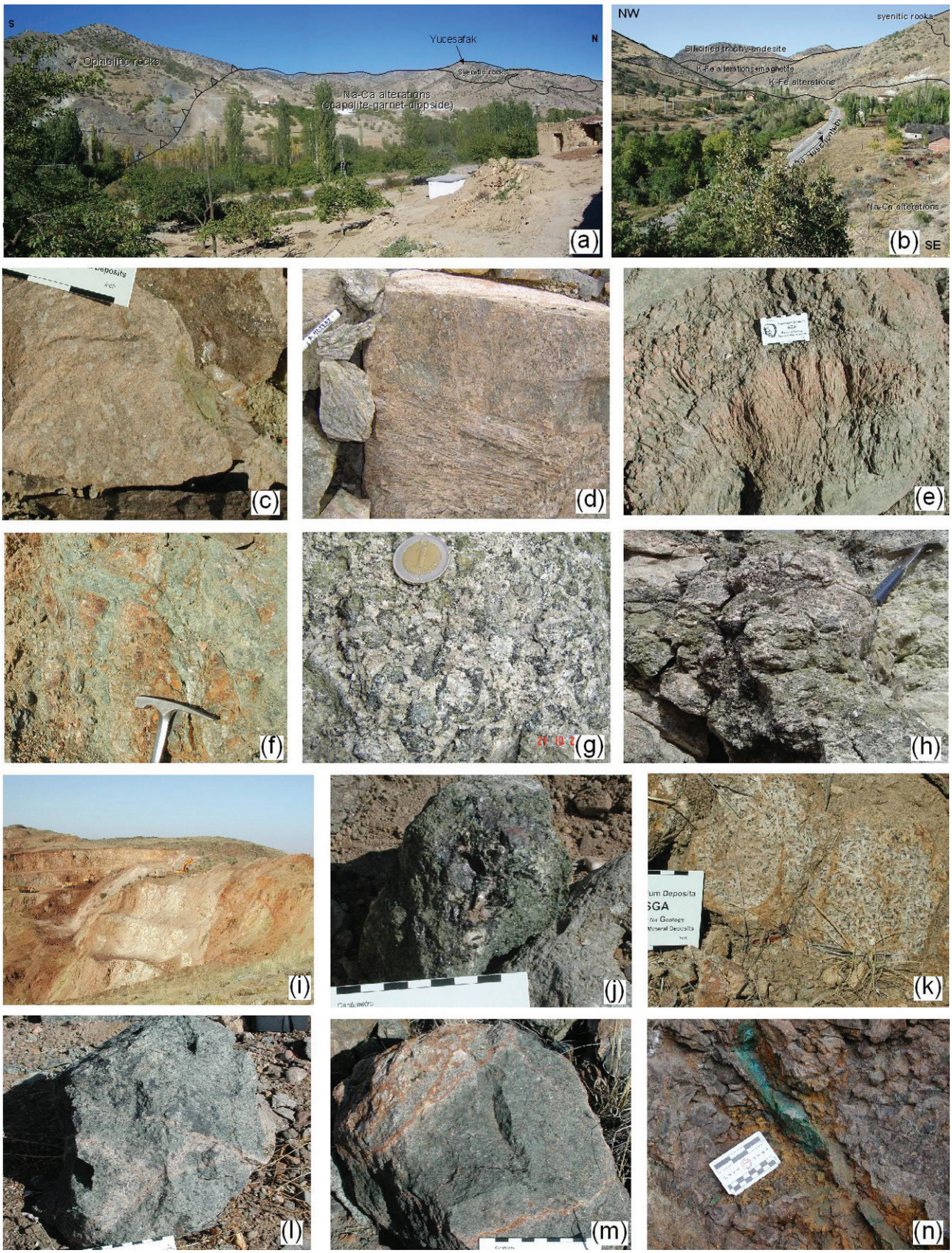

Figure 12: Main rock types, and their spatial association within the Hasançelebi deposit: **(a)** ophiolitic rocks along E-W trending strike-slip fault juxtaposing Na-Ca alteration with ophiolites; **(b)** field relationships between the alteration from south to north along koydere; **(c)** microsyenite porphyry; **(d)** coarse-scapolite crystals within syenite porphyry; **(e)** radiating crystals of pervasive scapolite in syenite porphyry; **(f)** scapolite-actinolite veins in trachytic rocks; **(g)** phlogopite replacing scapolite, note the unreplaced islands (light coloured rosette-like patches); **(h)** pervasive phlogopite replacing scapolite; **(i)** hematite-sericite-quartz alteration at Karakuz mine; **(j), (k)** and **(l)** calcite-quartz-pyrite veins in phlogopite rock with disseminated magnetite and epidote; **(m)** ankerite-quartz veins in phlogopite-magnetite rock; and **(n)** oxidised scapolite-actinolite rock and malachite staining along quartz-chalcopyrite vein.

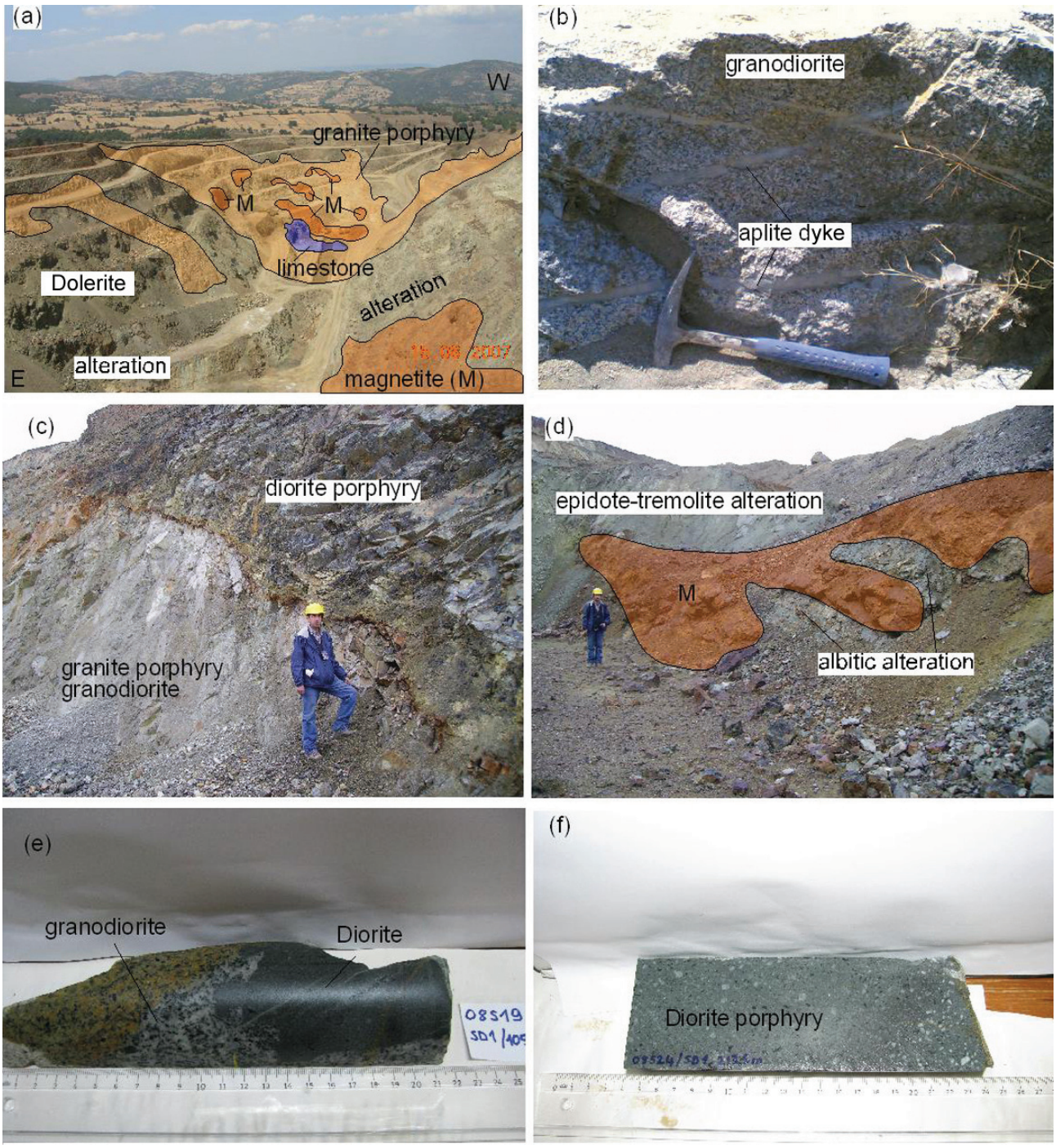

Figure 13: Main rock types, and their spatial association within the Şamlı deposit: **(a)** General view of the open-pit in the Şamlı deposit; **(b)** granodiorite-granite porphyry cut by aplite dykes; **(c)** contact between granite porphyry and diorite, and alteration along the contact zone; **(d)** magnetite vein within the syn-ore epidote-tremolite alteration overprinting the albitic alteration; **(e)** diorite enclaves within the granodiorite; and **(f)** diorite porphyry. M = magnetite.

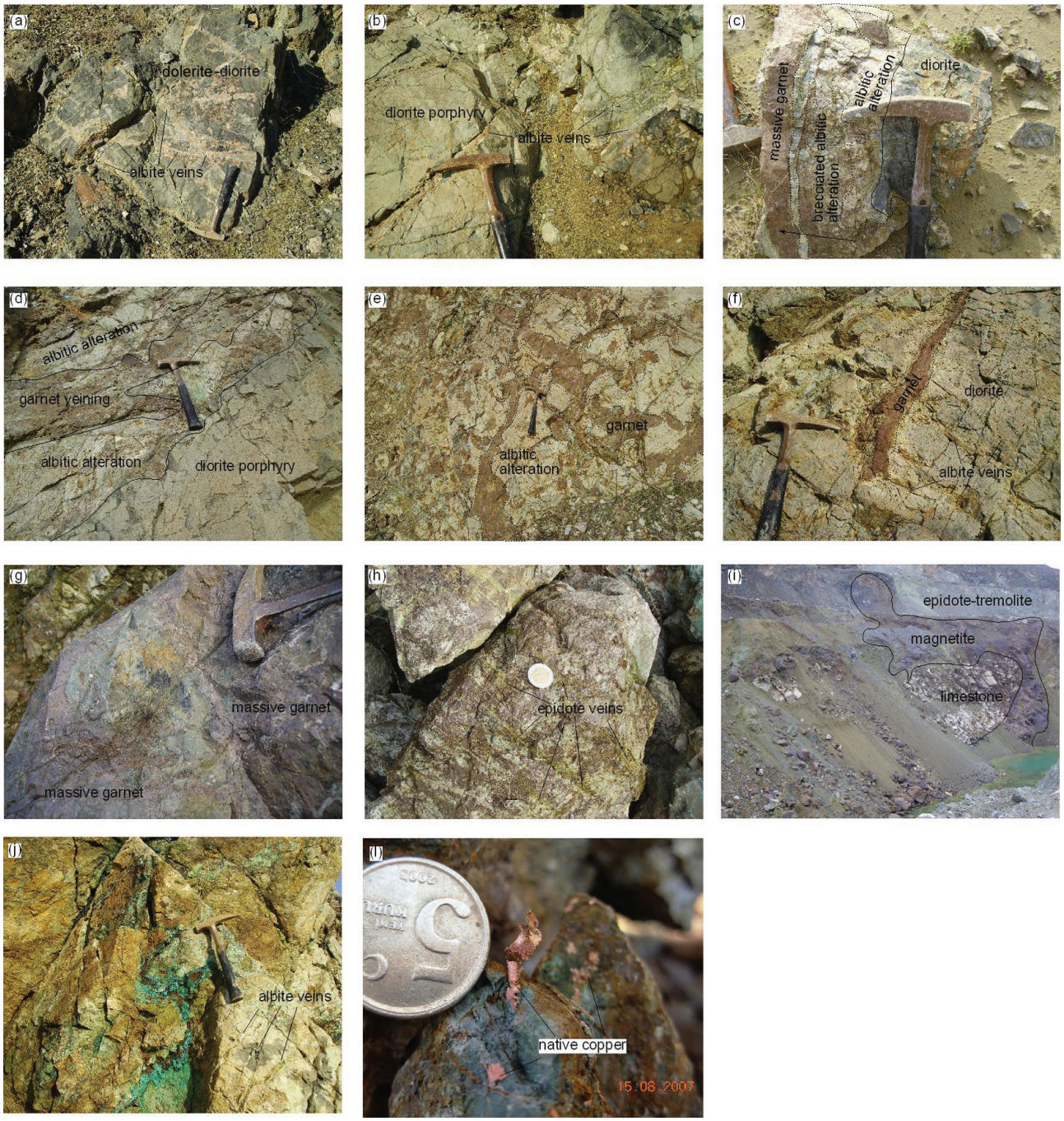

Figure 14: Characteristic features of hydrothermal alteration and magnetite ore from the Şamlı deposit: **(a)** albite veins within dolerite; **(b)** albitic alteration and albite veins within diorite porphyry; **(c)** albitic alteration, brecciation and superimposing garnet alteration within diorite, arrow shows the intensity of garnet alteration; **(d)** albitic alteration overprinted by garnet alteration within diorite porphyry; **(e)** garnet patches within the albitic alteration; **(f)** garnet vein cutting through albite veins; **(g)** massive garnet; **(h)** epidote veins overprinting the garnet alteration; **(i)** magnetite lens within syn-ore alterations; **(j)** malachite precipitation through the fractures within Na-Ca alteration; and **(k)** native copper.